

This is a repository copy of *Establishing Drug Discovery and Identification of Hit Series for the Anti-apoptotic Proteins, Bcl-2 and Mcl-1.*

White Rose Research Online URL for this paper:

<https://eprints.whiterose.ac.uk/146994/>

Version: Published Version

---

**Article:**

Murray, James B., Davidson, James, Chen, Ijen et al. (21 more authors) (2019) Establishing Drug Discovery and Identification of Hit Series for the Anti-apoptotic Proteins, Bcl-2 and Mcl-1. ACS Omega. pp. 8892-8906.

<https://doi.org/10.1021/acsomega.9b00611>

---

**Reuse**

[*"licenses\_typename\_other"* not defined]

**Takedown**

If you consider content in White Rose Research Online to be in breach of UK law, please notify us by emailing [eprints@whiterose.ac.uk](mailto:eprints@whiterose.ac.uk) including the URL of the record and the reason for the withdrawal request.

# Establishing Drug Discovery and Identification of Hit Series for the Anti-apoptotic Proteins, Bcl-2 and Mcl-1

James B. Murray,<sup>†,ID</sup> James Davidson,<sup>†</sup> Ijen Chen,<sup>†</sup> Ben Davis,<sup>†</sup> Paweł Dokurno,<sup>†,ID</sup> Christopher J. Graham,<sup>†</sup> Richard Harris,<sup>†</sup> Allan Jordan,<sup>†,ID</sup> Natalia Matassova,<sup>†</sup> Christopher Pedder,<sup>†</sup> Stuart Ray,<sup>†</sup> Stephen D. Roughley,<sup>†,ID</sup> Julia Smith,<sup>†</sup> Claire Walmsley,<sup>†</sup> Yikang Wang,<sup>†,ID</sup> Neil Whitehead,<sup>†</sup> Douglas S. Williamson,<sup>†,ID</sup> Patrick Casara,<sup>‡</sup> Thierry Le Diguarher,<sup>‡</sup> John Hickman,<sup>‡</sup> Jerome Stark,<sup>‡</sup> András Kotschy,<sup>§,ID</sup> Olivier Geneste,<sup>‡</sup> and Roderick E. Hubbard<sup>\*,†,II,ID</sup>

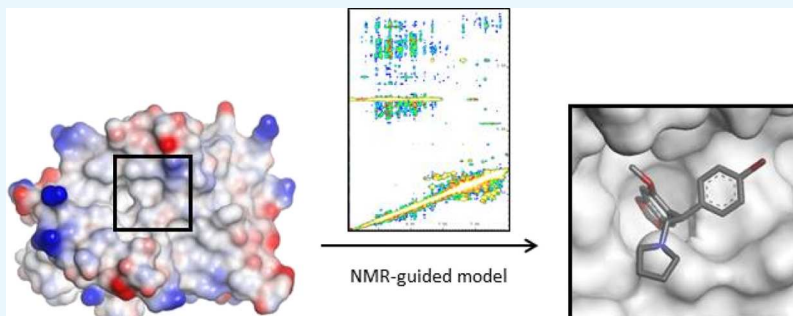
<sup>†</sup>Vernalis (R&D) Ltd., Granta Park, Abington, Cambridge CB21 6GB, U.K.

<sup>‡</sup>Institut de Recherches Servier Oncology R&D Unit, Croissy Sur Seine 78290, France

<sup>§</sup>Servier Research Institute of Medicinal Chemistry, Budapest 1031, Hungary

<sup>II</sup>YSBL, University of York, Heslington, York YO10 5DD, U.K.

## Supporting Information



**ABSTRACT:** We describe our work to establish structure- and fragment-based drug discovery to identify small molecules that inhibit the anti-apoptotic activity of the proteins Mcl-1 and Bcl-2. This identified hit series of compounds, some of which were subsequently optimized to clinical candidates in trials for treating various cancers. Many protein constructs were designed to identify protein with suitable properties for different biophysical assays and structural methods. Fragment screening using ligand-observed NMR experiments identified several series of compounds for each protein. The series were assessed for their potential for subsequent optimization using <sup>1</sup>H and <sup>15</sup>N heteronuclear single-quantum correlation NMR, surface plasmon resonance, and isothermal titration calorimetry measurements to characterize and validate binding. Crystal structures could not be determined for the early hits, so NMR methods were developed to provide models of compound binding to guide compound optimization. For Mcl-1, a benzodioxane/benzoxazine series was optimized to a  $K_d$  of 40  $\mu\text{M}$  before a thienopyrimidine hit series was identified which subsequently led to the lead series from which the clinical candidate S 64315 (MIK 665) was identified. For Bcl-2, the fragment-derived series were difficult to progress, and a compound derived from a published tetrahydroquinone compound was taken forward as the hit from which the clinical candidate (S 55746) was obtained. For both the proteins, the work to establish a portfolio of assays gave confidence for identification of compounds suitable for optimization.

## 1. INTRODUCTION

Mcl-1 and Bcl-2 are members of the family of Bcl-2-like proteins<sup>1</sup> that play a key role in regulating programmed cell death or apoptosis. The family consists of three classes of protein which contain between one and four of the so-called Bcl-2 homology domains (BH1–BH4). The pro-apoptotic class of protein such as Bax and Bak contains three BH domains that on activation form pores in mitochondria, triggering release of caspases leading to cell death. Activation is by a number of as-yet not fully characterized mechanisms but a major factor is relief of inhibition by binding to a class of single

BH3-only proteins such as Bim, Puma, Bad, Hrk, and Noxa. These BH3-only proteins bind variably to the well-characterized class of anti-apoptotic proteins Mcl-1, Bcl-2, and Bcl-x<sub>L</sub> (and less-studied Bcl-w and Bfl-1 or A1) which usually have four BH domains. These anti-apoptotic proteins are frequently upregulated in cancer cells, sequestering the BH3-only pro-apoptotic proteins, thus inhibiting apoptosis, and disruption of

Received: March 5, 2019

Accepted: March 8, 2019

Published: May 23, 2019

this interaction has been identified for a long time as a possible strategy for cancer therapy.

The Bcl-2 family represents a class of proteins for which it is challenging to generate drug-like molecules<sup>2</sup> because of the generally hydrophobic nature of the large protein–protein interaction surfaces to be disrupted. A number of other groups have reported success on these targets.<sup>3</sup> For Bcl-2, a series of clinical candidates eventually led to the marketed drug, ABT-199,<sup>4–6</sup> while a number of other groups report potent Mcl-1 inhibitors<sup>7–9</sup> some of which have entered clinical trials. We have recently disclosed compound series that inhibit Bcl-2<sup>10</sup> and Mcl-1,<sup>11</sup> and members of these series are now in clinical trials as a therapy for various cancers.

The first challenge faced for this class of target is to establish a robust drug discovery platform, including production of protein suitable for biophysical and functional assays, generating structural information and identifying tool compounds which can validate the assays that underpin hit identification and subsequent compound optimization. In this paper, we describe the development of structure-based discovery platforms for our Mcl-1 and Bcl-2 projects, which resulted in identification of the hit series of compounds which were subsequently optimized to clinical candidates. The structure-guided optimization of a thienopyrimidine series to cell-active inhibitors of Mcl-1 is described.<sup>12</sup> The optimization of other compounds will be described elsewhere.

**Figure 1** shows the structure we determined of the single helix of Bim bound into the groove provided by Mcl-1, similar

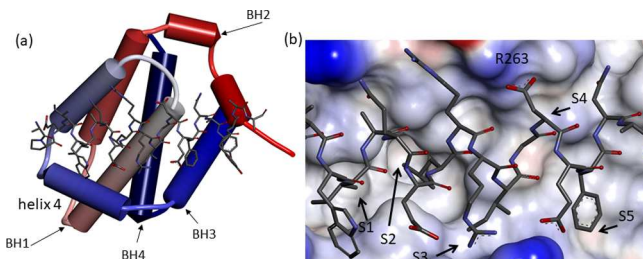


**Figure 1.** Crystal structure of the Bim peptide bound to hMcl-1. (a). Mcl-1 helical structure, colored from N (blue) to C (red) terminus, with the regions designated BH1–BH4 indicated, and with the Bim peptide in stick representation. (b). Details of the Bim peptide binding site on Mcl-1 with labels for the S1–S5 pockets and R263 of Mcl-1.

to that of the first published structure (pdb code: 2PQK<sup>13</sup>). This is architecturally similar to the complexes seen for other pro-apoptotic/anti-apoptotic pairs such as Bcl-x<sub>L</sub> with Bad (pdb code 1g5j) and summarizes the issue for generation of drug-like, potent inhibitors of the interaction which typically have subnanomolar affinities.<sup>14</sup> Mcl-1 has a large and predominantly hydrophobic cleft, characterized by a central charged amino acid (R263), flanked by a series of predominantly hydrophobic pockets, labeled S1–S5, which are occupied by the side chains of Bim.

The following sections describe the approach taken to generate the structure-based discovery platform for both Bcl-2 and Mcl-1 and the fragment and compound screening and characterization, which led to identifying hit series suitable for optimization for both the proteins. The description is organized with separate sections for each of the proteins under each method and activity. This is because there was considerable crossover between the projects in the develop-

ment of the methods and identification of initial hit compounds. The experimental methods are described in the section at the end of the manuscript with additional details including compound synthesis in the [Supporting Information](#).

## 2. RESULTS

**2.1. Generation of Suitable Protein—Bcl-2.** Early structural work on Bcl-x<sub>L</sub><sup>15</sup> by a group at Abbott characterized a long flexible loop between residues 28–80, connecting helices 2 and 3 in structures determined by both NMR spectroscopy and X-ray crystallography. This loop can be truncated with no effect on the function or structure. Bcl-2 has an equivalent long flexible loop. Work by the same Abbott group<sup>16</sup> found that intact Bcl-2 is not sufficiently soluble for structural studies but designed a Bcl-2/Bcl-x<sub>L</sub> hybrid for two isoforms of Bcl-2 (hereafter, Bcl-2#1 and Bcl-2#2), where the loop is shortened with a Bcl-x<sub>L</sub> sequence. Structures were reported for these Bcl-2 proteins determined by NMR spectroscopy.<sup>16</sup>

We generated Bcl-2#2 but found it was expressed in low yields and had poor stability in our hands, giving variable behaviors in NMR experiments. Modification of the screening buffers [to 50 mM MES/bis-TRIS pH 7.0, 20 mM Arg/Glu, 2 mM dithiothreitol (DTT)] provided a more stable protein which was used in initial NMR experiments and for surface plasmon resonance (SPR). However, we were not able to obtain crystals of Bcl-2#2 and a more stable protein was required for more extensive and routine NMR experiments.

Comparison of the sequence of Bcl-2#2 with Bcl-x<sub>L</sub> and its crystal structure identified a number of surface and C-terminal residues which could have an impact on protein behavior and crystallization. Modifications to these residues (shown in **Figure 2**) gave a construct we call Bcl-2#3 which was expressed in high yield. This construct had a similar selectivity profile for BH3-only peptides as wild-type Bcl-2 and weak interaction with the Bcl-x<sub>L</sub>-specific peptide Hrk (**Table S1**). Bcl-2#3 was stable at 800 μM for 2–3 weeks at 30 °C, suitable for structural studies by both NMR spectroscopy (<sup>15</sup>N labeled and <sup>15</sup>N, <sup>13</sup>C labeled) and X-ray crystallography. In addition, the protein showed slow exchange on the NMR timescale when binding potent ligands, with evidence of the increased order (see **Figure S1**). A further modified version was produced (Bcl-2#3'), in which some surface glutamic acids were modified (to alanine or glutamine) to remove some carboxylate/carboxylate interactions seen in crystal packing, and this was used for one of the crystal structures reported here (2 in **Figure 3**); subsequent work on advanced compounds derived from 2 showed the same binding mode in other Bcl-2 constructs.<sup>10</sup> Unmodified human Bcl-2 residues 1–207 with an N-terminal hexa-His tag and a thrombin cleavage site (hereafter hBcl-2) was produced for assays.

**2.2. Generation of Suitable Protein—Mcl-1.** The first crystal structures of Mcl-1 were published in 2007 (PDB code: 2NL9<sup>17</sup>) as we began our work on Mcl-1. Mouse Mcl-1 (hereafter mMcl-1) was more soluble than human Mcl-1 (hereafter hMcl-1), and a number of mouse mutations were introduced into hMcl-1 for this structure. We introduced further nine mutations to vary surface residues and alter the pI of the protein and the length of the N and C termini. This eventually led to the protein we term hMcl-1#1 (with an N-terminal GST tag and 3C protease cleavage site), which was used to determine some initial crystal structures with pro-apoptotic peptides bound (a cartoon representation of the

	20	30	90	100	110			
(a)	<i>Bcl-2#2</i> : MAHAGRTGYDNEIVMKYIHYKLSQRGYEWADGVVEENRTEAPEGTESEVVHLLRQAGDFDSRRYRQLFAEMS							
	<i>Bcl-2#3</i> : MSQ-----DNRREVVKMYISYKLQRGYEWADGVVEENRTEAPEGTESEVVHQLTLRQAGDFDSRLYRQLFAEMS	*						
		*****	*****	*****	*****			
	120	130	140	150	160	170	180	190
	<i>Bcl-2#2</i> : SQLHLTFPTARGRFATVVEELFRDGVNWRGIVAFTEFFGVMVCESVNREMSPLVDNIALWMTXLNHLHTWIQ							
	<i>Bcl-2#3</i> : SQLHLTPGTAYASFATVVEELFRDGVNWRGIVAFTEFFGVMVCESVNREMSVLVDNIAAWMATYLNDHLHTWIQ	*						
		*****	*****	*****	*****	*****	*****	*****
	200							
	<i>Bcl-2#2</i> : DNGGWDADFVELYPGPSMR							
	<i>Bcl-2#3</i> : DNGGWDADFVELYGNNAAESRGQERFLE	*****	*****	*****	*****	*****	*****	*****
		*****	*****	*****	*****	*****	*****	*****
	180	190	200	210	220	230	240	
	<i>mMcL-1</i> : DDLYRQSLEIIISRYLREQATGSKDSPKLGEAGAAAGRRALETLRVRGVGDGVQRNRHETAFQGMRLRKLDIKNEGDVKS							
	<i>hMcL-1</i> : DELYRQSLEIIISRYLREQATGAKDTKPMGRSGATSRKALETLRVRGVGDGVQRNRHETAFQGMRLRKLDIKNEGDVKS	*						
		*****	*****	*****	*****	*****	*****	*****
	<i>2NL9</i> : DDLYRQSLEIIISRYLREQATGS-----GAAGRALETLRVRGVGDGVQRNRHETAFQGXLRLKDIDKNEDDVKS							
	<i>hMcL-1#1</i> : DDLYRQSLEIIISRYLREQATGAKDTKPMGRSGATSRKALETLRVRGVGDGVQRNRHETAFQGMRLRKLDIDKNEDDVKS							
		*****	*****	*****	*****	*****	*****	*****
	250	260	270	280	290	300	310	
	<i>mMcL-1</i> : FSRVMVHFVFKDGVNTNWGRIVTLLSFGAFVAKHLKSVNQESIEPIELAETITDVLVRTKRDWLVKQRGWGDFGVFF							
	<i>hMcL-1</i> : LSRVMVFSDGVNTNWGRIVTLLSFGAFVAKHLKTIQNQESIEPLAESITDVLVRTKRDWLVKQRGWGDFGVFF	*						
		*****	*****	*****	*****	*****	*****	*****
	<i>2NL9</i> : LSRVXIHVFSGDGVNTNWGRIVTLLSFGAFVAKHLKTIQNQESIEPLAESITDVLVRTKRDWLVKQRGWGDFGVFF							
	<i>hMcL-1#1</i> : FSRVMVHFVFKDGVNTNWGRIVTLLSFGAFVAKHLKSVNQESIEPLAETITDVLVRTKRDWLVKQRGWGDFGVFF							
		*****	*****	*****	*****	*****	*****	*****
(b)	320							
	<i>mMcL-1</i> : HVQDLEGG							
	<i>hMcL-1</i> : HVEDLEGG	*						
		*****	*****	*****	*****	*****	*****	*****
	<i>2NL9</i> : HV							
	<i>hMcL-1#1</i> : HVQDLEGG							

**Figure 2.** Amino acid sequence of (a) Bcl-2—a comparison of the Bcl-2#2 sequence used to generate PDB entry 2o21 and used here for fragment screening and initial NMR experiments and the sequence designed for the Bcl-2#3 construct, which was used for X-ray crystallography, SPR, and most NMR experiments. Sequence numbering is for human Bcl-2. Highlighted in green is the loop which is not seen in the crystal structure and identity between the two sequences is indicated with \*; a construct with reduced surface charge (Bcl-2#3') was used for some X-ray crystallography with E to A mutations at positions marked in pink except for E114Q (FAEM > FAQM) (b) Mcl-1—a comparison of the sequence seen in the crystal structures of Bim bound to the modified Mcl-1 in PDB entry 2NL9 with hMcl-1, mMcl-1, and hMcl-1#1. Sequence numbering is for human Mcl-1. \* signifies sequence identity between hMcl-1 and mMcl-1. The sequence differences between 2NL9 and hMcl-1 are highlighted in pink and the differences between hMcl-1 and hMcl-1#1 in blue. X is seleno-methionine. Full sequences (including tags) are in the [Supporting Information](#).

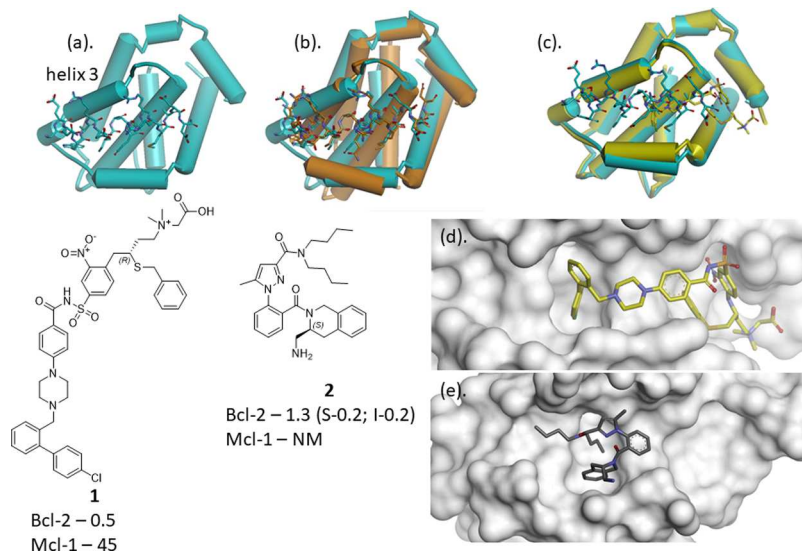


**Figure 3.** Bcl-2#3 crystal structures: (a) Bcl-2#3 bound to Puma; (b) structure of Puma bound to Bcl-2#3 (blue) and hMcI-1 (orange), overlaid on Puma; (c) Structure of Bcl-2#3 bound to Puma (blue) and **1** (yellow); (d) detail of binding of **1** (yellow); and (e) detail of binding of **2** (grey) to Bcl-2#3'.

structure of hMcl-1#1 bound to the BH3-only peptide Puma is shown in Figure S2). We then found that sufficient quantities of soluble hMcl-1 could be generated with no mutations, by swapping to an N-terminal hexahis tag and either a TEV or thrombin cleavage site. This hMcl-1 was used for subsequent crystallographic studies, fragment screening, and various assays and initial  $^1\text{H}$  and  $^{15}\text{N}$  heteronuclear single-quantum correlation (HSQC) NMR experiments. In addition, a double his-tagged version was produced for SPR,<sup>18</sup> which was also suitable for isothermal titration calorimetry (ITC). However, the lack of long-term solubility of hMcl-1 precluded its use for routine  $K_d$  determination using  $^1\text{H}$ ,  $^{15}\text{N}$  HSQC experiments, and so mMcl-1 was used. Figure 2b compares the sequence in

PDB code 2NL9<sup>17</sup> with that of mMcl-1, hMcl-1, and hMcl-1#1.

### **2.3. Assays To Validate Binding of Compounds to**

**Proteins.** In addition to the 1D  $^1\text{H}$  NMR methods used in ligand-observed NMR fragment screening described below, four different assays were developed to validate or characterize binding of compounds to Bcl-2 or Mcl-1 during this hit identification phase: fluorescence polarisation (FP),  $^1\text{H}$ ,  $^{15}\text{N}$  HSQC NMR, ITC, and SPR. Details of the reagents and protocols are provided in the [Experimental Section](#), in brief:

**2.3.1. FP Assays.** Ligand binding was measured from the change in FP on displacement of the BH3-only peptide, F-

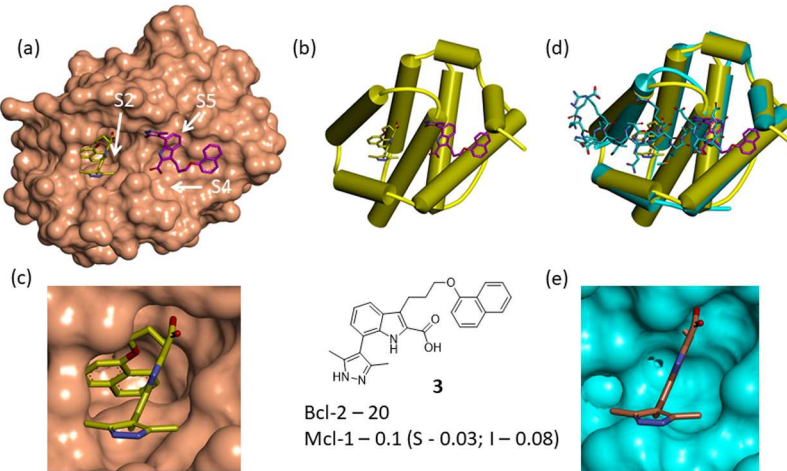


**Figure 4.** hMcl-1 crystal structures: (a,b) structure of compound 3 bound to two sites on hMcl-1 with (c). Detail of binding of 3 that binds in the S2 pocket; (d) comparison of hMcl-1 structures with 3 (yellow) and Puma (blue) bound with (e). Detail of the hMcl-1 binding surface for Puma overlaid in blue on the observed binding position of 3 in the S2 pocket. The convention for the assay data is summarized in the legend to Figure 3.

Puma (Puma peptide N-terminally labeled with a fluorescein analogue), using hBcl-2 or hMcl-1.

**2.3.2.  $^1\text{H}$  and  $^{15}\text{N}$  HSQC NMR.** This 2D NMR experiment on an  $^{15}\text{N}$  isotopically labeled protein sample generates a peak for each amide with a chemical shift highly sensitive to the chemical environment near that particular amide group. Typically, spectra are acquired for 30–50  $\mu\text{M}$  protein with increasing concentration of the ligand, limited only by the solubility of the ligand. Clearly defined peaks for most amides indicate a homogenous and soluble protein sample with binding of the ligand to a defined site, giving a titration of movement of peaks of amides in the binding site (e.g., Figure S1) from which  $K_{\text{d}}$  can be estimated if saturation can be achieved. The initial HSQC NMR experiments used hMcl-1 and subsequent experiments used the more soluble and stable mMcl-1.

**2.3.3. Isothermal Titration Calorimetry.** Experiments were conducted, where compounds have sufficient solubility, at 25 °C by titration of a stock sample of the 100  $\mu\text{M}$  compound onto a solution of 10  $\mu\text{M}$  hMcl-1 in a GE ITC200 instrument. The lower solubility of later compounds sometimes required titration of the protein onto the compound.<sup>10</sup>

**2.3.4. Surface Plasmon Resonance.** A direct binding method was used, in which the protein (his-tagged Bcl-2#2 or hMcl-1 with a double his-tag<sup>f8</sup>) was immobilized on an NTA chip on a Biacore T100 instrument. Serial dilutions of the ligand were then made to flow over the surface, with regeneration of the surface between each sample. A competition or “affinity in solution” method was developed later for optimized compounds for both Mcl-1<sup>11</sup> and Bcl-2,<sup>10</sup> in which variable concentrations of the ligand with a fixed concentration of protein are made to flow over an SPR chip with a potent ligand bound (either the peptide or optimized compound). This format of SPR assay was not used for the compounds referenced here.

**2.4. Bcl-2 Structural Information—X-ray Crystallography.** Although there were crystal structures of various BH3-only peptides binding to Mcl-1 and Bcl-x<sub>L</sub> when we began our project, there were no published structures determined by either NMR spectroscopy or X-ray crystallography of such peptides binding to Bcl-2. We determined the crystal structure of Bcl-2#3 bound to the BH3-only peptide, Puma, and

compared it with a structure we determined of Puma bound to hMcl-1 (Figure 3). There is an overall similarity in the binding mode of Puma, with some small variation in the relative orientations of the various helices that form the peptide binding cleft.

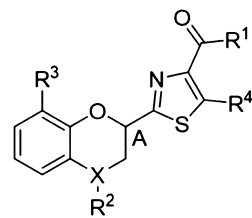
Data shown for all compounds in this paper are  $\mu\text{M}$  values for  $eK_i$  for FP assay for that target [with data in brackets for measurements of  $K_{\text{d}}$  by HSQC NMR (N), SPR (S), or ITC (I) where available], unless the assay curve is incomplete, when it is expressed as percentage inhibition at the highest concentration. NM—not measurable at the concentrations used in the assay (for FP—2.5 mM or solubility limit).

We could only crystallize Bcl-2#3 in the presence of a high affinity ligand. Therefore, we were not able to determine structures with the early hit series from fragment screening. The first crystal structure we determined of a small molecule binding to Bcl-2#3 was with compound 1, an analogue of ABT-737 (Figure 3d). This binds with a very similar pose to that seen for the then-published structure of ABT-737 in Bcl-x<sub>L</sub> (pdb code: 2YXJ<sup>19</sup>).

**2.5. Mcl-1 Structural Information—X-ray Crystallography.** Similar to our experience with Bcl-2#3, we could only determine the structures of hMcl-1 in complex with peptides or small molecules with potency better than 100 nM, and the success rate for cocrystallization was low. In the latter stages of our Mcl-1 project, more routine crystal structure determination was achieved with a maltose binding protein (MBP)-Mcl-1 fusion (as described elsewhere<sup>11</sup>), but this was not available at the time of the studies reported here.

Figure 4 shows the crystal structure of hMcl-1 bound to the indole acid compound 3, a tool compound derived from a patent but reinforced by an indole acid fragment hit (see later). Two copies of the ligand occupy the binding cleft. The ligand in S2 is binding into a deep pocket that is not present in the Puma-bound structure (Figure 2e). The ligand centered on S4 is between two molecules in the crystal packing environment, which we believe is an artifact of crystallization as ITC experiments demonstrate binding with 1:1 stoichiometry, and the poor enclosure of the ligand in S4 makes it unlikely to be a relevant pocket. The binding affinity of 3 for hMcl-1 is 100 nM  $eK_i$  in the FP assay, consistent with ITC and SPR data (see Figure S3), with selectivity of about 300-fold over Bcl-2.

Table 1. Optimisation of the Benzodioxane/Benzoxazole Series



Cmpd	R1	R2	R3	R4	X	A <sup>1</sup>	Mcl-1 <i>eKi</i> <sup>2</sup> (μM)	Mcl-1 <i>Kd</i> <sup>3</sup> (μM)	Bcl-2 <i>eKi</i> <sup>4</sup> (μM)
15	-NMe <sub>2</sub>		H	H	O		NM	2600	NM
21	-OH		H	H	O		40	280	300
22 <sup>5</sup>	-OH		H	CH <sub>2</sub> Ph	O		40	85 (S-140)	80 (N-210)
23	-OH	H	H	H	N		500	360	NM
24	-OH	Et	H	H	N		20	220	500
25	-OH	CH <sub>2</sub> Ph	H	H	N		40	40 (S-450)	800 (N-210)
26	-OH	CH <sub>2</sub> Ph	H	H	N	R	30	110	NM
27	-OH	CH <sub>2</sub> Ph	H	H	N	S	40	140	NM
28 <sup>5</sup>	-OH	CH <sub>2</sub> Ph	Me	H	N	R	47	70	93

<sup>a</sup>NM—not measurable at top concentration tested, usually 2.5 mM or solubility limit;<sup>1</sup> a blank means the racemic compound was tested;<sup>2</sup> *eKi* (μM) is measured by Mcl-1 FP assay;<sup>3</sup> *Kd* is measured by <sup>1</sup>H, <sup>15</sup>N HSQC (S is *Kd* measured by SPR);<sup>4</sup> *eKi* is measured by Bcl-2 FP assay (μM unless incomplete assay curve, when expressed as percentage inhibition at the top concentration), N is *Kd* measured by <sup>1</sup>H, <sup>15</sup>N HSQC;<sup>5</sup> and NGM is generated.

These structures demonstrate that there is conformational flexibility in both the proteins (more in Bcl-2 than in Mcl-1), where both side-chain and main-chain movements can adjust the surface of the protein to accommodate changes in the ligand. These movements can substantially change the nature of the binding surface, revealing additional pockets that increase the “druggability”<sup>20</sup> of the protein.

**2.6. Identifying and Characterizing Fragment Hits—Bcl-2.** The initial NMR experiments on Bcl-2 were acquired with the Bcl-2#2 protein at 10 μM. A total of 1088 fragments were screened as mixtures of 8 (with each compound at 500 μM). The initial analysis suggested 82 hits, with a hit defined as showing competition with the 30 μM Puma peptide in three ligand-observed NMR experiments [saturation transfer difference spectroscopy (STD), water-LOGSY, and Carr–Purcell–Meiboom–Gill]. However, there was some variability and ambiguity in assigning hits because of protein instability giving low signal to noise in the experiments. The initial set of hits were remeasured in the ligand-observed experiments as singletons and with a single-point and <sup>1</sup>H, <sup>15</sup>N titration HSQC experiments, resulting in 24 validated hits which could be grouped into 5 structural classes (Figure S4).

At this point in the project, the Bcl-2#3 protein had been obtained for X-ray crystallography. This showed increased stability and was adopted for all subsequent studies.

**2.7. Identifying and Characterizing Fragment Hits—Mcl-1.** The initial fragment hits came from two sources. First, the 1064 fragments in the library at that time were screened at 500 μM each compound as mixtures of 8 against 10 μM hMcl-1 using ligand-observed NMR with 25 μM Noxa-B peptide as the competitor. A total of 39 fragments were confirmed when retested as singletons as competitive in all three NMR experiments and fall into 13 different classes (Figure S5). Second, building on the observation that biaryl acids are often found as binding to this type of protein–protein interaction surface,<sup>21</sup> commercially available analogues of two biaryl acids (**4** and **5**) were assessed, and from this, the pyrazolo-acid **6** was identified. Any compounds that were hits were also assessed by

<sup>1</sup>H, <sup>15</sup>N HSQC NMR experiments and tested in the hMcl-1 FP assay.

**2.8. NMR-Guided Models.** We were unable to determine the structures for fragment hits binding to either Bcl-2 or Mcl-1 by X-ray crystallography. Instead, we used an approach that we refer to as NMR-guided models (NGMs). This technique is suitable for proteins with a molecular weight up to around 35 kDa, with either a full assignment or partial assignment (sometimes achieved with selective labeling of particular amino acid types). The Experimental Section describes the methods in detail, but in summary, the spectrum of the ligand is assigned in the bound state using <sup>13</sup>C, <sup>15</sup>N purged 1D and nuclear Overhauser spectroscopy (NOESY) experiments. A full 3D <sup>13</sup>C-edited, <sup>13</sup>C, <sup>15</sup>N-filtered NOESY (so-called X-filtered NOESY) is then acquired, which identifies intermolecular NOEs between the ligand and protein. These restraints are then used to filter ligand poses from docking into an ensemble of protein conformations.

For each of Mcl-1 and Bcl-2, an ensemble of protein conformations (including movement of side chains in the putative ligand binding sites) was generated from the then available structures (determined by X-ray crystallography or NMR) supplemented by analysis of molecular dynamics (MD) simulation and homology models. For Mcl-1, only peptide-bound crystal structures were available, but a homology model based on the available ligand-bound Bcl-2 structures and the simulation suggested movement of helix 4. For Bcl-2, both ligand and peptide-bound structures were available, and the simulation suggested movement of helix 3. The compound of interest was then docked into all enumerated protein conformations and the three docking models that best satisfied the observed NOEs were subjected to an induced-fit docking protocol. The docking models from fixed-protein and induced-fit docking were examined side by side to select a final model.

As crystal structures could be determined for larger compounds such as **2** for Bcl-2 and **3** for Mcl-1, we generated an NGM of **2** with Bcl-2 and **3** with Mcl-1 and compared these to the X-ray structures (Figure S6). This confirmed that the

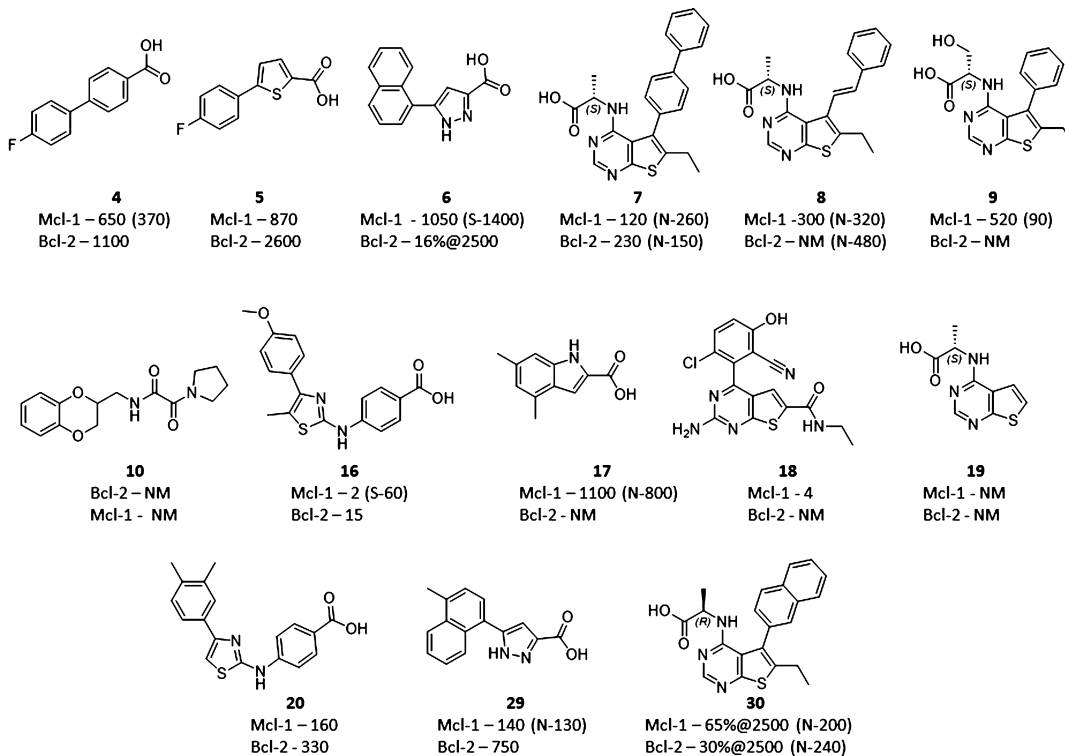


**Figure 5.** Compounds referenced in this paper (see also Table 1 and other figures). The convention for the assay data is summarized in the legend to Figure 3.

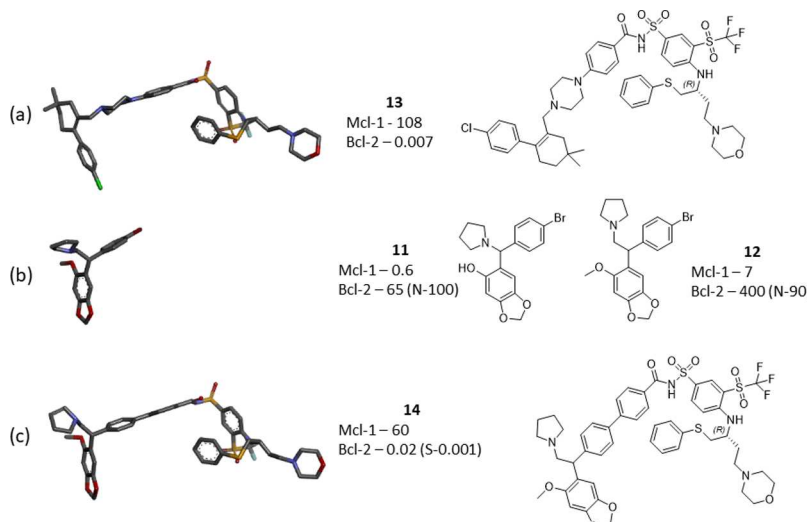


**Figure 6.** Design of the hybrid Bcl-2 compound showing on the left the experimentally determined pose (Bcl-2 protein structure omitted) for each of (a) crystal structure of ABT-263, **13**; (b) NGM model of binding of benzodioxole, **12**, and (c) crystal structure of the hybrid compound, **14**. The convention for the assay data is summarized in the legend to Figure 3.

NGM can provide an adequate model for compound optimization for both the proteins.

**2.9. Hit Identification—Bcl-2.** A number of fragment series were explored for Bcl-2 and representatives of the hit series emerging for Mcl-1 (see later). The affinity for Bcl-2 of various fragments and fragment-derived series was low (see Table 1 and Figure 5) and there was no selectivity for Bcl-2 over Mcl-1, so the series were not progressed further for Bcl-2. However, a number of thienopyrimidines (such as **7**, **8**, **9**) were identified in the near neighbor screening, which showed emerging SAR and selectivity for Mcl-1 (see later).

It was striking that a number of benzodioxanes were identified for both targets, such as **10**. The Mcl-1 project also identified benzodioxoles such as **11** (see later) and limited SAR identified **12** with an affinity of 67  $\mu$ M for Bcl-2#3 by  $^1\text{H}$ ,  $^{15}\text{N}$  HSQC and with suitable physicochemical properties such that an NGM could be determined for binding to Bcl-2#3. This collection of results suggested that such a semisaturated fused-ring system could occupy the S2 pocket in Bcl-2. We also determined the crystal structure of the then-leading candidate for Bcl-2 (ABT-263<sup>S</sup>, **13**) and realized, as shown in Figure 6, that piperazine of **13** overlays with the bromobenzene in **12**,

suggesting that chlorobenzene of **13** could be replaced by benzodioxole of **12**. This hybrid compound (**14**) was synthesized and it binds with an affinity of around 1 nM (FP data confirmed by SPR, data in *Figure S1*), although it has only weak cellular activity (data not shown) and was not pursued further. However, the crystal structure of **14** bound to Bcl-2#3 (*Figure 6c*) confirms that the design strategy was correct and provides further confirmation that the NGM approach does generate poses for small molecules that can be exploited in synthesis.

After exploring the various fragments and hit series for nearly a year, a publication from UCB<sup>22</sup> revealed tetrahydroisoquinoline amide substituted phenyl pyrazoles as potent and selective Bcl-2 inhibitors. A novel representative of the series, **2**, was synthesized, characterized, and the crystal structure bound to Bcl-2#3 was determined (*Figure 3c*). This provided the hit series, which was subsequently optimized to a clinical candidate,<sup>10</sup> through a structure-guided design that will be described elsewhere.

**2.10. Hit Identification—Mcl-1.** It is challenging to evolve fragments in the absence of detailed structural information, so the initial exploration for Mcl-1 aimed to generate SAR through assessment of near neighbors of the hits identified from fragment screening that were available in the Vernalis in-house library. This library is held on 96-well plates and where more than 20 near neighbors were present, the whole plate was screened. In total, over 2000 compounds were screened and four hit series emerged: benzodioxanes such as **15**; aminothiazoles as exemplified by **16** (a serendipitous hit from screening a plate of compounds); pyrazolo acids exemplified by **6** (a near neighbour of indole acid fragment hits such as **17**), and the thienopyrimidine series which were fragment hits for both Mcl-1 and Bcl-2 (**7–9, 18, 19**). Preliminary exploration of the SAR around these series was informed by the structural models for binding derived from the NGMs (see *Figure 7*).

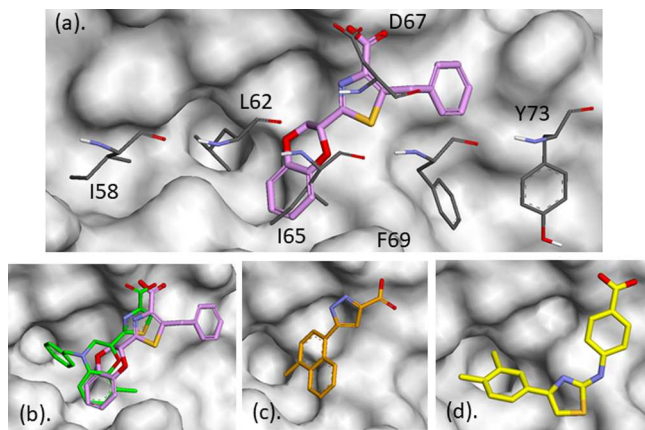


**Figure 7.** hMcl-1 NGM structures: molecular surface of the Mcl-1 structure used to generate models of compound binding with (a) selected amino acid side chains of BIM from the 2NL9 structure shown in stick with grey carbon atoms with the NGM-derived pose of the R-enantiomer of benzodioxane **22** (purple) (the model of the S-enantiomer was identical except for slight rearrangement of the benzodioxane moiety); NGM-derived pose of (b) benzoxazine **28** in stick with green carbon atoms superposed on **22**; (c) pyraloacid **29** with orange carbons; and of (d) aminothiazole **20** with yellow carbons.

**2.10.1. Benzodioxane/Benzoxazines.** Analogues of benzodioxane fragment **15** were explored by purchase or synthesis, leading to the optimized benoxazine **20** as summarized in *Table 1*. Although **15** had very weak affinity for Mcl-1, the carboxylic acids, such as **21**, were more potent, and an NGM was generated for the analogue **22**. The model (*Figure 7a*) suggests dioxane is not making specific interactions, and a nitrogen atom (i.e. benzoxazine) could offer a vector into the S2 pocket. Although oxazine **23** binds more weakly than its equivalent dioxane, **21**, introduction of an ethyl (**24**) and then benzyl (**25**) gave increased potency with no preference for R (**26**) compared to S (**27**) stereoisomer. Additional modifications explored around the benzene moiety of the benzoxazine and an NGM was generated for one of the most potent compounds, the R enantiomer **28**, demonstrating the success of the NGM model in the guiding design. However, limited progress was made in improving the ligand efficiency. Other bicyclic compounds such as benzodioxole **11** were identified under the NIH PubChem initiative from a fluorescence resonance energy transfer-based uHTS conducted to identify inhibitors of the Mcl-1/NOXA or Mcl-1/Bid interaction at the Emory University Molecular Libraries Screening Centre (bioassay 1021 and 1022 in <https://pubchem.ncbi.nlm.nih.gov/bioassay>). **11** had some selectivity for Mcl-1 over Bcl-2 but poor behavior in biophysical assays. The benzoxazine and benzodioxole series of compounds were not pursued further for Mcl-1.

**2.10.2. Aminothiazoles.** There were aminothiazole-containing fragment hits (such as **15**—which was classified as a benzodioxane series member), but the series actually developed from analysis of near neighbors of other fragment hits and from serendipitous hit identification during whole-plate screening in the near neighboring process. Compound **16** is a typical representative of the series which had reasonable potency and generated an NGM. A number of analogues were explored synthetically, but the series was not progressed because of poor physicochemical properties (mainly solubility), with modifications to improve solubility, leading to a rapid drop in ligand efficiency.

**2.10.3. Pyrazoloacids.** The commercially available pyrazoloacids were investigated and for one (**29**), an NGM was obtained, which reinforced the emerging hypothesis that the acidic moiety binds to R263, anchoring the compound with an aromatic group pointing toward the S2 pocket. However, the series was not progressed as most of the compounds had poor solubility and so were difficult to characterize.

**2.10.4. Indole Acids.** The fragment screen identified a number of indole (and related fused ring) acids as hits for Mcl-1. In addition, a patent from Abbott reported indole acids from an HTS screen<sup>23</sup> (subsequently optimized to potent Mcl-1 compounds<sup>24</sup>). A number of analogues were synthesized, including **3**, which had sufficient potency to give a crystal structure (*Figure 4*) and showed some selectivity for Mcl-1 over Bcl-2. This provided a compound that could be used to validate the structural biology and biophysical assays for the project. However, as well as not being novel, the series showed very high plasma protein binding and so was not pursued further.

**2.10.5. Thienopyrimidines.** The initial screen of the Vernalis compound collection for near neighbors of fragment hits (as described above) was performed before the Bcl-2 project was underway and identified some thienopyrimidines (such as **18** and **19**) with activity in the FP assay. However,

this series was not pursued initially as other series looked more promising. When the additional thienopyrimidines were identified in the Bcl-2 project, it was found that this series had tractable SAR, selectivity, and opportunities for optimization against Mcl-1. The thienopyrimidines were therefore adopted as the lead series, and the optimization from the initial hit to a cell-active, high-affinity, and selective Mcl-1 inhibitor is described elsewhere.<sup>12</sup>

### 3. DISCUSSION

The discovery of the hit compounds that led to the Servier/Vernalis clinical candidates for each of the Bcl-2<sup>10</sup> and Mcl-1<sup>11</sup> proteins provides an example of how structure-based drug discovery can be enabled for the challenging task of inhibiting a protein–protein interaction. The approach taken requires the extension and integration of established techniques from across many different disciplines such as protein production, assay development, biophysical measurement of protein–ligand interactions, X-ray crystallography, and NMR spectroscopy.

The essential requirement for any structure-based drug discovery approach is the production of protein material suitable for a range of biophysical and functional assays. At the time we initiated our Mcl-1 and Bcl-2 projects, there were published constructs that had been successfully used for NMR-based structural-based discovery for Bcl-2<sup>6</sup> and some preliminary structural studies of Mcl-1.<sup>17</sup> These published constructs did not have the required stability or solubility in our hands, and so, a number of modifications were made. For Bcl-2, the main improvement came from structure-guided modification of the surface of the protein to alter physical properties, using information from available crystal structures of the more tractable homolog, Bcl-x<sub>L</sub>. The Mcl-1 project required more substantial protein engineering. Although variations in the purification tag (and cleavage approach) generated human Mcl-1 (hMcl-1) protein suitable for FP assay and crystallography, the protein did not have the solubility and stability required for the longer timescale of <sup>1</sup>H, <sup>15</sup>N NMR experiments, and so, mouse Mcl-1 (mMcl-1) was used.

The biophysical and structural methods used in these early hit identification studies included a number of mutations in the protein to improve properties such as solubility, stability, and crystallization. Although SAR was mainly derived from the FP assay against the wild-type protein, there is a danger that these mutations might lead to anomalies in the biophysical or structural data generated. For Bcl-2, the profile of binding to different BH3-only peptides (Table S1) gave confidence that the Bcl-2#3 construct was appropriate for the biophysical assays. The difference in sequence between mouse and human Mcl-1 was not considered for the early hit compounds reported here. This was an issue for compounds later in optimization (9-fold higher affinity for a published compound in human vs mouse<sup>11</sup>), probably because of the L246F mutation which affects compounds binding deep into the S2 pocket. However, this interaction is not exploited in the early hit compounds.

The use of several assay formats can aid establishing reliable measurements of affinity for the interaction of weakly binding compounds to proteins such as Mcl-1 and Bcl-2 where there are large hydrophobic clefts, which could promote poor compound behavior. For example, we found considerable variability in the measurement of affinity using an early version of the FP assay with values that were inconsistent with measurements by other biophysical methods. Each of the assay

formats has different dynamic ranges and different requirements for the protein construct, for the behavior of the compound and protein in solution (solubility, aggregation) and the amount of the reagent required. Most of the cross-validation of binding during hit identification and hit optimization used <sup>1</sup>H, <sup>15</sup>N HSQC measurements of affinity (to a  $K_d$  of around 10  $\mu\text{M}$ ) with either ITC or SPR used to measure binding affinity of more potent compounds to these proteins.<sup>10,11</sup> The <sup>1</sup>H, <sup>15</sup>N HSQC measurements are the most robust as they directly measure the protein and ligand state. Each experiment confirms the solubility and concentration of the protein and ligand, the folded state of the protein and the integrity of the ligand. In addition, the measurements can give an indication of which site the ligand is binding to. There are varying issues with the other assay formats, including spectral interference with the FP assay, solubility for ITC, and solubility and nonspecific binding to the chip surface, giving non-stoichiometric responses for SPR. Such anomalies can be particularly acute for low-affinity compounds. The consistency of compound behavior in the assays was one of the contributing factors to selecting thienopyrimidines as hits to be progressed for Mcl-1.

A number of groups have reported<sup>25–28</sup> on how the number of hits from a fragment screen provides an indication of the intrinsic ability of the protein to bind small molecules (sometimes referred to as druggability; the phrase ligandability is more appropriate<sup>29</sup>). The earliest example of this is from the Abbott group.<sup>26</sup> Our own analysis of fragment screening campaigns some years ago<sup>25</sup> highlighted that a low hit rate in fragment screening gave an indication of how difficult it would be to identify lead-like compounds for a target. As discussed in that paper,<sup>25</sup> this could be due to the nature of the protein interaction surface (such as the essentially flat, hydrophobic cleft of  $\beta$ -catenin, PPI-3 in that paper) or the intrinsic flexibility of the binding site, providing an entropic penalty for any ligand binding such as for the ATPase site on Hsp70. The number of validated fragment hits for Bcl-2 (24) and Mcl-1 (39) is higher than the number which could be anticipated for a fairly large, hydrophobic cleft. However, the NGMs (e.g., Figure 6) suggest that many of the hits exploit the charged residue in the center of the cleft (R146 for Bcl-2 and R263 for hMcl-1), as confirmed in subsequent crystal structures. The difference in the hit rate from the fragment screen between the two targets could be due to different intrinsic flexibilities and ligandability of the proteins. There are indications from crystal structures that Bcl-2 is more flexible than Mcl-1. The root-mean-square deviation (rmsd) for least squares overlap on main chain atoms for the published crystal structure of Bcl-2 bound to BAX (PDB code: 2XA0) compared to the structure bound to S 55746 (6GL8<sup>10</sup>) is 3.6 Å; this contrasts with an rmsd of 1.7 Å for Mcl-1 bound to Bim (2NL9) compared to the structure bound to S 63845 (5LOF<sup>11</sup>). The challenge of identifying lead candidates may also be reflected in the different numbers of reported clinical candidates (including our own series, 2 for Bcl-2<sup>4</sup> and at least 5 for Mcl-1<sup>7,9,30</sup>).

The crystal structure of Bcl-x<sub>L</sub> was determined some time ago,<sup>15</sup> and it was our experience (not reported here) that we were able to determine many crystal structures of this BH3 family protein in complex with both pro-apoptotic peptides and with various ligands. However, there remain relatively few published crystal structures for Bcl-2. The early drug discovery relied on NMR structure determination,<sup>16</sup> and it was our experience that crystal structures with small molecule ligands

were only obtained once high affinity binding had been achieved (as shown in **Figure 3**, see also ref 10). For Mcl-1, it was relatively straightforward to obtain crystal structures with peptides bound (as shown in **Figures 1** and **3**), but again crystallization of the native hMcl-1 complexed with small molecules required high-affinity ligands.<sup>11</sup> For both proteins, we were unable to obtain crystals of the apo protein, perhaps because the ligand was required to stabilize a conformation of the protein which crystallized. One recent innovation is to fuse Mcl-1 with MBP.<sup>31</sup> This stabilizes the protein and generates crystals with the ligand binding pocket available for soaking of ligands. Using a similar strategy, we were able to obtain many crystal structures of MBP-Mcl-1 with both low- (**Figure S6**) and high-affinity<sup>11</sup> compounds bound.

As discussed, the early structure-based design work at Abbott on Bcl-2 relied on structures determined by NMR spectroscopy. Such NMR structures require considerable effort in labeling with multiple isotopes (<sup>2</sup>H, <sup>13</sup>C, <sup>15</sup>N), the collection of many 2D NMR spectra, and the time-consuming assignment of each peak in the spectrum to individual nuclei. Once assigned, NOE experiments can then identify specific protein–protein and protein–ligand interactions from which a full structure determination can be achieved. This takes some time and in addition, optimization of the ligand can lead to changes in the spectrum which require reassignment to be performed. We adopted an NGM approach. This begins with generating computational models that reflect the possible conformations for the protein and a cascade of rigid followed by flexible docking protocols to generate putative binding poses for the ligand in the protein binding site. The NMR experiments do not require full assignment but generate sufficient information to identify which nuclei in the ligand are interacting with which nuclei on the protein. These distances are then used to select the model for the ligand binding to the protein from the docking poses.

The NGM approach was initially validated by the compound design illustrated in **Figure 6**. The NGM of a fragment-derived compound (**11**) was used to design a high-affinity compound (**14**) which merged the fragment with part of an established Bcl-2 binding motif (**13**). The subsequent crystal structure confirmed that the NGM had successfully identified the correct binding mode for **11**. NGMs were generated for the various hit series for Mcl-1 and can assist in optimization, as shown for the benzodioxane to benzoxazine optimization in **Figure 4b**. However, there are limits to the extent to which the NGM binding modes can be used to rationalize observed affinity and selectivity. An NGM was generated for the thienopyrimidine **30** binding to Bcl-2. As can be seen in **Figure S6**, there is a significant difference in the binding pose of the central thienopyrimidine motif seen in this NGM compared to that seen in the later determination of the crystal structure of the closely related compound, **9**, determined in MBP-hMcl-1 (note that the pose of the thienopyrimidine core in **9** was retained into the optimized compounds such as S 63845<sup>11</sup>). It may be that compounds binding with around 200 μM (**30**) to 500 μM (**9**) affinity do adopt different conformations, for example, to accommodate the additional aromatic ring in the naphthalene of **30** and the NGM is reporting an incorrect pose, or the change in orientation is due to differences between Mcl-1 and Bcl-2 in this pocket. Because of this uncertainty, it was difficult to provide a structural rationale for the consistent selectivity for Mcl-1 over Bcl-2 seen for the initial thienopyrimidine series. However, the initial SAR for this

series (described elsewhere<sup>12</sup>) was sufficient to guide early optimization without the support of structural information.

The fragment screening against each of the targets identified several hit series. The consistent feature in most of the fragment hits for both of the proteins is a negative charge which binds the charged arginine side chain in Mcl-1 (R263) or Bcl-2 (R146), which “anchors” the compound as seen in **Figures 4** and **7**, and this is retained in the optimized compounds such as **1** for Bcl-2 and S 63845<sup>11</sup> for Mcl-1. However, the fragment hit **11** demonstrates that small uncharged compounds can bind to Mcl-1, as also seen for the early hit **2** binding to Bcl-2 and retained in the optimized compound S 55746.<sup>10</sup> Although the initial fragment hits did not lead directly to the lead compounds for either of these targets, the experience with the fragments allowed the assays and platform to be established and validated, such that good quality hits could be recognized when they become available.

## 4. CONCLUSIONS

We have demonstrated how the combination of biophysical and structural methods enabled structure-based discovery platforms to be built for each of the Bcl-2 and Mcl-1 proteins. Such target enablement is increasingly a barrier to establish drug discovery for many of the recently proposed target classes identified by modern “omics” technologies. Also, as well as the increasing number of protein–protein interaction targets,<sup>2</sup> similar challenges exist for large multidomain, multiprotein complexes and intrinsically disordered proteins. Establishing such a platform can take some time and resource—a tool compound is usually needed to validate the assays, but the assays are needed to identify the tool compound. However, such investment is needed to identify compounds of sufficient potency, selectivity, and cellular activity to demonstrate whether inhibition (or activation) delivers the expected effect on the biology of the system. The thienopyrimidine series provided compounds which characterize the effect of Mcl-1 inhibition on cells.<sup>11,12</sup>

## 5. EXPERIMENTAL SECTION

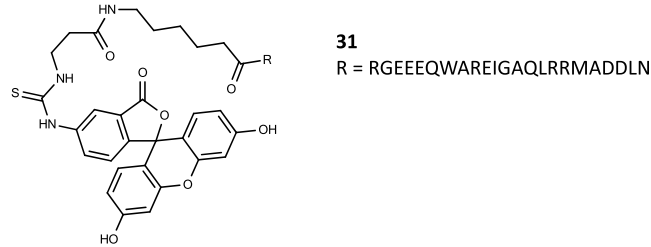
**5.1. Materials.** Peptides were obtained from Biopeptide LLC. The peptide F-Puma (**31**) was used for assays.

Puma has the sequence RGEEEQWAREIGAQLRRMADDLN

Puma-S has the sequence EEEQWAREIGAQLRRMADD

Peptide Bim has the sequence DMRPEIWIAQELRRIGDEFWAYYARR

Peptide Noxa-B has the sequence PADLKDECAQLRIGDKVNL



**5.2. Methods.** **5.2.1. Protein Production—Bcl-2.** Codon-optimized genes encoding respective Bcl-2 proteins were synthesized (DNA2.0, now ATUM) and ligated to pET28a (Bcl-2#2) or pET21a (Bcl-2#3 and hBcl-2) between the NdeI

and XhoI sites. The sequences of the proteins are given in the Supporting Information.

**5.2.2. Expression of *Bcl-2* Proteins.** *Escherichia coli* BL21 (DE3) pLysS cells were transformed with respective *Bcl-2*-encoding plasmid and cultured at 37 °C in 10 flasks each containing 1 L Luria–Bertani (LB) supplemented with 50 µg/mL of kanamycin (for *Bcl-2#2*) or 100 µg/mL of ampicillin (for *Bcl-2#3* and h*Bcl-2*). Once the culture had reached an OD<sub>600</sub> of 0.6, 1 M IPTG was added to each flask to induce expression (1 mM final concentration). The cells were pelleted after 16 h at 18 °C via centrifugation (10 000 rcf, 20 min) and stored at –80 °C. For the production of labeled protein for NMR studies, complex M9 media supplemented with <sup>13</sup>C-labeled D-glucose and/or <sup>15</sup>N-labeled ammonium sulphate was used instead of LB.

**5.2.3. Purification of *Bcl-2* Proteins.** Cell pellets were resuspended in 200 mL of lysis buffer (50 mM Tris-HCl, 500 mM NaCl, 0.5 mM DTT, 10% (w/v) glycerol, and pH 8.0) containing Roche Complete ethylenediaminetetraacetic acid (EDTA)-free protease inhibitor cocktail and DNase I (Sigma). The resuspended cells were lysed by mechanical homogenization. The lysed cells were centrifuged (41 000 rcf, 60 min) and the supernatant was applied to a 5 mL of HisTrap FF column (GE Healthcare) using an AKTA FPLC system (GE Healthcare). Column-bound protein was washed with lysis buffer containing 25 mM imidazole and then eluted with lysis buffer containing 500 mM imidazole. The eluted protein was then applied to a HiLoad 26/60 Superdex 200pg column (GE Healthcare) in sizing buffer (20 mM Tris-HCl, 200 mM NaCl, 2 mM EDTA, 1 mM DTT, and pH 8.0) and stored at –80 °C.

**5.2.4. Protein Production—*Mcl-1*.** Human *Mcl-1* (h*Mcl-1*) and mouse *Mcl-1* (m*Mcl-1*) were generated by gene synthesis (Celtek BioScience, TN, USA/ATUM, CA, USA). h*Mcl-1#1* was generated by a DNA shuffling technique of fragments from h*Mcl-1* and m*Mcl-1*. These genes were introduced into a number of different expression vectors as listed in the Supporting Information.

**5.2.5. Expression of *Mcl-1* Proteins.** The *Mcl-1* constructs were expressed in *E. coli* BL21 (DE3) pLysS. For material that required isotopic labeling, EPBNF (EnPresso, Germany) or M9 media was supplemented with <sup>15</sup>N (NH<sub>4</sub>)<sub>2</sub>SO<sub>4</sub> and/or <sup>13</sup>C D-glucose (CIL, MA, USA).

**5.2.6. Purification of the MBP-h*Mcl-1* Protein.** The expression and purification of this protein are described elsewhere.<sup>11</sup>

**5.2.7. Purification of Other *Mcl-1* Proteins.** Purification involved either Ni<sup>2+</sup> affinity followed by ion-exchange/size-exclusion chromatography or initial capture by GST affinity chromatography. Where needed, the resulting protein was incubated with either PreScission protease (GE Healthcare, USA) or thrombin to yield untagged proteins. Cleaved material was further purified by either ion-exchange or size-exclusion chromatography.

**5.2.8. NMR Experiments to Characterize Binding.** All NMR spectra were acquired at 298 K on a Bruker AVANCE 600 MHz spectrometer with either a TCI or a QCI-F cryogenically cooled probe, including a z-axis pulse-field gradient coil. Dissociation equilibrium constants (*K*<sub>D</sub>) of compounds were determined by monitoring the chemical shift perturbations from the acquisition of a series of 2D <sup>1</sup>H, <sup>15</sup>N HSQC spectra with increasing compound concentration and analyzed with MNova Binding (MNova, Mestrelab Research, Santiago de Compostela, Spain) using a single binding site

model. Titrations were acquired on 50 µM m*Mcl-1* in MES pH 6.0 buffer or 20 mM Tris pH 7.8, 50 mM NaCl, 2 mM DTT, and on 30–40 µM *Bcl-2#3* in 50 mM Tris, pH 7.5.

**5.2.9. Assignment/NOE Detection for NGMs.** The backbone and side-chain resonances of apo *Bcl-2#3* (concentration and buffer) and apo m*Mcl-1* (concentration and buffer) were achieved using three-dimensional HNCO, HNCA, HN(CA)-CB, CBCA(CO)NH, and HBHA(CBCACO)NH and HCCH-TOCSY experiments and analyzed using CCPN Analysis.<sup>32</sup> For each NGM, the HSQC titration was followed to achieve saturation of the protein with the ligand. For ligands in slow to medium exchange, the collection of three-dimensional experiments were performed to reassign the spectra. For ligands in fast exchange, the resonance assignments were extrapolated from those of the apo protein by comparing two-dimensional <sup>1</sup>H, <sup>13</sup>C HSQC spectra at increasing ligand concentrations. Ligand–protein NOEs were detected from a 3D <sup>1</sup>H, <sup>13</sup>C-edited, <sup>13</sup>C/<sup>15</sup>N-filtered NOESY acquired with a mixing time of either 120 or 150 ms on 200 µM m*Mcl-1* in 50 mM MES/bistris pH 6.0 or 200 µM *Bcl-2#3* in 20 mM MES/bistris pH 7.4.

**5.2.10. Calculation of NGMs for *Mcl-1*.** Molecular modeling was conducted either with the molecular operating environment (MOE) (<http://www.chemcomp.com>) or Schrodinger (<http://www.schrodinger.com>) suites of software. Analysis of the available BH3 public structures upon project inception already suggested a significant conformational change between a peptide bound compared to a compound-bound BH3 protein. However, there were only peptide-bound *Mcl-1* structures at the time this project was started. To address the possibility of protein flexibility, we first carried out an MD simulation of *Mcl-1* (details below), and then, a protein conformational ensemble was prepared for *Mcl-1* for NGM derivation. When enumerating such ensemble of conformations, we focused particularly on movements of helix 4 suggested by the internal MD simulation analysis of *Mcl-1* and also the side chain orientations of the residues involved in the NOEs. In addition, to expand the diversity of protein conformations, homology models based on ligand-bound *Bcl-2/Bcl-x<sub>L</sub>* structures were built and added to the ensemble. The compound of interest was then docked into all enumerated protein conformations. The resulting docking models were visually inspected, and the best three docking models in terms of satisfying the observed NOEs were then subjected to the induced-fit docking protocol. A set of docking models from fixed-protein and induced-fit docking was examined side by side to nominate a final model.

**5.2.11. *Mcl-1* MD Simulation.** The published structure of h*Mcl-1* bound to BIM (pdb code 2PQK<sup>13</sup>) was chosen to start the MD simulation for *Mcl-1*. The missing loop connecting helix 1 and helix 2 was rebuilt with MOE guided by the structure of m*Mcl-1* bound to NOXA the peptide (pdb code 2JM6<sup>33</sup>). The rebuilt *Mcl-1* protein was prepared using Schrodinger's Protein Preparation Wizard,<sup>34</sup> which added hydrogens, assigned appropriate protonation and rotamer states for residues, and performed restrained minimization. The simulation system of apo h*Mcl-1* (starting from BIM bound conformation) was built with the Schrodinger's Maestro interface in the NPT ensemble, with explicit TIP3P waters and counter ions added to neutralize the overall charge of the system. The default setup parameters were kept unless mentioned specifically here. Periodic boundary conditions were applied, and long-range electrostatic interactions were

treated with Ewald sums.<sup>35</sup> The MDs were performed with Desmond<sup>36</sup> at a constant temperature (300 K) and pressure (1.01 bar), and coordinates were saved every 4.8 ps, keeping the default settings. The AMBER ff98SB force field<sup>37</sup> was used for a 50 ns simulation. The simulation results were analyzed with tools from Schrodinger and MOE. A set of diverse conformations and 2PQK were included in the final protein conformational ensemble for NGM enumeration.

**5.2.12. Mcl-1 Homology Models Based on Bcl-2/Bcl-x<sub>L</sub>.** The experimental ligand-bound Bcl-x<sub>L</sub> structures (pdb codes: 2O1Y, 2O2F, 2O21, 2W3L and 2YXJ) and ligand-bound Bcl-2 structure (compound 1) were used as templates. The sequence alignments and model building were performed using MOE with AMBER ff99 force-field<sup>37</sup> and generalized Born solvation.<sup>38</sup> Up to 10 main-chain models were built for each template.

**5.2.13. Docking Details for Mcl-1.** Prior to docking, compounds were prepared with LigPrep from Schrodinger and docking grids were generated by Glide<sup>39,40</sup> on all protein conformations. The default parameters were used. Compounds were modeled in each of the protein conformations using the Glide SP protocol from Schrodinger, generating up to 10 poses while everything else was kept at default. The selected docking models with reasonable NOE matching were subjected to Schrodinger's Induced-Fit docking protocol.<sup>41</sup> All the resulting docking models were visually inspected to propose a final model.

**5.2.14. Computational Work for Bcl-2 NGMs.** The approach used to enumerate Bcl-2 NGMs is similar to that described for Mcl-above. One difference was the availability of ligand-bound Bcl-x<sub>L</sub> experimental structures at the time of the project. Bcl-x<sub>L</sub> is highly analogous to Bcl-2 in sequences, and the bound ligands also inhibit Bcl-2. This allows construction of Bcl-2 ligand-bound homology models, which enhances the diversity of the protein conformational ensemble but also allows for anticipating Bcl-2 flexibility in a more defined manner. The available experimental structures suggest that the main flexibility of Bcl-x<sub>L</sub> and likely for Bcl-2 comes from helix 3 upon ligand binding. Therefore, we explored helix 3 mobility when generating a Bcl-2 conformational ensemble. The compound of interest was subjected to the same docking protocol as Mcl-1, fixed-protein followed by induced-fit docking. Inspection of selected docking poses led to final models used for medicinal chemistry.

**5.2.15. Bcl-2 Ligand Bound Homology Models.** The experimental ligand-bound Bcl-x<sub>L</sub> structures (PDB codes: 1YSG, 1YSI, 1YSN, 2O1Y, 2O2F, 2O2M, 2O2N, 2O21, 2O22, 2W3L, and 2YXJ) were extracted from PDB to use as templates. The alignments and model building were performed using MOE with AMBER ff99 force-field<sup>37</sup> and generalized Born solvation.<sup>38</sup> Up to 10 main-chain models were built for each template. A ligand-bound Bcl-2 X-ray structure (compound 1) was later determined internally which validated the homology model approach.

**5.2.16. Docking Details for Bcl-2.** Prior to docking, compounds were prepared with LigPrep from Schrodinger and docking grids were generated by Glide<sup>39,40</sup> on selected Bcl-2 protein conformations with default parameters. The Glide SP protocol in the Schrodinger suite was employed to model compounds in selected Bcl-2 protein conformations, generating up to 10 poses per compound per protein conformation. The docking models with reasonable NOE matching were subjected to Schrodinger's Induced-Fit docking protocol.<sup>41</sup> All

the resulting docking models were visually inspected to propose a final model.

**5.3. Assays.** **5.3.1. F-Puma Assay.** The assays were carried out in black-walled, flat-bottomed, low binding, 384-well plates. Compound [final conc. 5% dimethyl sulfoxide (DMSO)] was mixed in buffer (10 mM 4-(2-hydroxyethyl)-1-piperazineethanesulfonic acid, 150 mM NaCl, 0.05% Tween 20, and pH 7.4), containing 10 nM compound 31 (F-Puma) and either 10 nM His-TEV-hMcl-1 or hBcl-2. Assay plates were incubated ~2 hours at room temperature and FP measured on a Synergy 2 reader (Ex. 528 nm, Em. 640 nm, cut off 510 nm). The binding of increasing doses of compound was expressed as a percentage reduction in mP compared to the window established between "DMSO-only" and "total inhibition" controls (10–30 μM Puma). The inhibitory concentrations that gave a 50% reduction in mP ( $IC_{50}$ ) were determined, from an 11-point dose response curves, in XL-Fit using a 4-Parameter Logistic Model (Sigmoidal Dose–Response Model).  $K_i$  was subsequently calculated as previously described.<sup>42</sup> All FP data reported in this publication are the average of at least three determinations. For most compounds, the standard deviation in  $eK_i$  values were within 15% of the average; for some, the standard deviation was 40%.

**5.3.2. Isothermal Titration Calorimetry.** Double His-tag TEV hMcl-1 was dialyzed prior to use in 2 L of 50 mM Phosphate, 50 mM NaCl, 0.5% MTG (v/v) 1 mM EDTA at pH 7.4 for 3 h at room temperature. The protein was dialyzed using a 3.5 K molecular weight cut-off Slide-A-Lyzer cassette. The protein solution was recovered, spin-filtered through a 0.22 μM frit, and the resulting protein quantified by UV absorbance at 280 nm using an extinction coefficient of 20 970 M<sup>-1</sup> cm<sup>-1</sup>. 500 mL of dialysis buffer was retained (remainder used to rinse out SCHOT bottle) and degassed for a minimum of 30 min under vacuum with constant stirring. Experiments were performed on a GE ITC200 instrument. 100 μM compound was titrated from the syringe into the cell containing 10 μM protein. The solutions were carefully matched to ensure same solvent and buffer conditions were present in both the syringe and cell (this is to minimize heat of dilution effects). The final solution was the dialysis buffer plus 1% DMSO. The experiment was performed over 25 injections with stirring at 1000 rpm, gain setting high, and at 25 °C. Pure water was used in the reference cell. The first injection was 0.4 μL with a duration of 1 s with a gap of 150 s until the further 24 injections of 1.6 μL with a duration 6.1 and a 240 s interval between injections. Data were analyzed using the vendor supplied software, PEAQ-ITC Analysis Software. The data model used was the single site model. The data shown are the average of two independent experiments.

**5.3.3. SPR—Direct Binding.** Experiments were carried out on a Biacore T100 instrument (GE Healthcare) at 25 °C in HBS-P buffer at pH 7.4 supplemented with 1 mM TCEP and 1% DMSO. Single his-tagged Bcl-2#2 or double His-TEV-hMcl-1 proteins were immobilized on Series S NTA chips. The surface in the experimental channel was consecutively treated with 500 μM NiCl<sub>2</sub> and 50 nM protein. Reference surfaces without immobilized Ni<sup>2+</sup> served as controls for nonspecific binding and refractive index changes. The protein surface was regenerated between experiments with 0.35 M EDTA and 40% DMSO (both for 1 min, 15 μL min<sup>-1</sup>). Serial dilutions of the compound in the running buffer were injected over the surface. All sample measurements were performed at a flow rate of 30 μL min<sup>-1</sup>. Data processing was performed using BIAevaluation

1 (BIAcore GE Healthcare Bio-SciencesCorp) software. Sensorgrams were double-referenced prior to global fitting of the concentration series to a 1:1 binding model.

**5.4. Fragment Screening.** The Vernalis fragment library of approximately 1000 compounds<sup>43</sup> was screened in mixtures of eight compounds per sample on a Bruker DRX600 equipped with a BACS-120 sample changer. Mcl-1 samples contained 10  $\mu\text{M}$  hMcl-1 protein and 500  $\mu\text{M}$  of each compound, in 20 mM tris pH 7.4 50 mM NaCl, 100  $\mu\text{M}$  DTT, and 10% D<sub>2</sub>O. Bcl-2 samples contained 12  $\mu\text{M}$  Bcl-2#2 and 500  $\mu\text{M}$  of each compound in 50 mM tris pH 7.5, 50 mM NaCl, 250  $\mu\text{M}$  DTT, 500  $\mu\text{M}$  EDTA, and 10% D<sub>2</sub>O. <sup>1</sup>H 1D, STD,<sup>44</sup> the water ligand observed via gradient spectroscopy (waterLOGSY),<sup>45</sup> and relaxation-filtered spectra<sup>46</sup> were acquired on all samples under ICONNMR automation, using excitation sculpting to suppress the solvent peak. Excitation sculpting used 2 ms square pulses with  $\gamma\text{B}_1/2\Pi \approx 250$  Hz. A spectral width of 12 376 Hz was used in all experiments, and all experiments were acquired at 298 K. Competition was determined by addition of the 25  $\mu\text{M}$  NoxaB peptide (Mcl-1) or 500  $\mu\text{M}$  Puma peptide (Bcl-2), following acquisition of the set of NMR experiments for each sample, in order to confirm specific binding at or near to the active site. Data were analyzed as described previously<sup>47</sup>—the spectra were analyzed manually and competitive hits confirmed as singletons.

**5.5. X-ray Crystal Structure Determination.** **5.5.1. Crystallisation of Bcl-2.** The hBcl-2#3 protein was used for the crystal structure of Bcl-2 complexed with compounds **1**, **13**, and **14**, and hBcl-2#3' was used for compound **2**. In all cases, the protein was initially complexed with the ligand by mixing protein (4 mg/mL, 0.2 mM in 20 mM Tris buffer pH 8.0, 0.2 M NaCl, and 1 mM DTT) with 10-fold excess of compound from 200 mM stock DMSO solution and incubated at 4 °C for 1 h and then concentrated to about 9 mg/mL (0.4 mM) before being used for crystallization with commercial screens. For Bcl-2 in complex with compound **1**, crystals appeared after four weeks in a droplet containing 1.4 M sodium/potassium phosphate, pH 5.6. The bipyramidal crystal (with edge of ~0.2 mm) was immersed in cryo-protection solution (1 M Na/K phosphate pH 5.6, 30% glycerol) and flash-frozen in liquid nitrogen. For Bcl-2 in complex with Puma-S, crystals appeared overnight and grew up to ~0.2 mm in the longest dimension over the following three days. Crystals grown from 0.2 M MgCl<sub>2</sub>, 25% PegMME 2k, 0.1 M Na acetate buffer pH 5.5 were prepared for data collection by cryo-protection (immersion in mother liquor enriched in Peg1k by 10%) and flash-frozen in liquid nitrogen. For Bcl-2 in complex with compound **2**, crystals were obtained from 0.2 M Ca acetate, 15% Peg4k, and 0.1 M Tris pH 7.5. Crystals were harvested, cryoprotected (immersion in mother liquor enriched in Peg1k by 20%), and flash-frozen in liquid nitrogen. For Bcl-2 in complex with **13**, crystals appeared overnight in a droplet containing 0.2 M NaCl, 25% Peg3350, and 0.1 M Bis-Tris buffer pH 5.5. Bipyramidal crystal was immersed in cryo-protection solution (70% crystallisation buffer, 30% glycerol) and flash-frozen in liquid nitrogen. For Bcl-2 in complex with **14**, crystals were grown from solution containing 0.15 M KSCN, 20% Peg1500, and 0.1 M Na acetate buffer pH 5.5.

**5.5.2. Crystallisation of Mcl-1.** The hMcl-1 protein was used for determination of the structure with BIM. Mcl-1 solution at ~10 mg/mL was mixed with 10-fold excess of the BIM peptide (water solution) and incubated overnight at 277 K. The formed complex was used for crystallization as

described in 2NL9.<sup>17</sup> (0.2 M Zn acetate, 0.2 M Imidazole pH 5.75, room temperature). hMcl-1#1 was used for the structure with Puma. Mcl-1 solution at ~10 mg/mL was mixed with 10-fold excess of the Puma peptide (water solution) and incubated overnight at 277 K. The formed complex was mixed with equal volume of the crystallization reservoir (0.1 M imidazole pH 7.0, 0.1 M Zn acetate, 25% Peg3350, 5% ethylene glycol) in a hanging drop, vapor diffusion technique. Elongated needles appeared overnight and were harvested in 2–4 days. MBP-hMcl-1 was used for the determination of the structure of **9** bound to Mcl-1. Structure determination was performed as described elsewhere<sup>11</sup> for S64385 bound to MBP-hMcl-1 PDB code SLOF). His-thrombin-hMcl-1 was used for structure determination with **3**. Crystals were grown in solution containing equal parts of protein solution (~5–10 mg/mL) mixed an appropriate compound (with 3–5 fold excess) and crystallization reservoir solution (1.8 M ammonium citrate pH 7.0) in the hanging drop format of the vapor diffusion technique, using 24-well Linbro plates.

**5.5.3. X-ray Data Collection.** Suitable crystals for data collection were flash-frozen in liquid nitrogen after cryoprotection using the crystallization reservoir enriched in ethylene glycol (Mcl-1) and Peg1k or glycerol (Bcl-2). Table S2 summarizes the data collection statistics, with data obtained from ESRF and dynamic light scattering synchrotrons or single crystal X-ray diffraction equipment consisting of rotating anode generator RUH300 coupled with a Raxis-IV++ image plate detector (Rigaku MSC instrument installed at Vernalis, Cambridge, UK). Data were processed and scaled with DENZO/Scalepack package<sup>48</sup> for all structures except Bcl-2 with **30** which used d\*TREK.<sup>49</sup>

**5.5.4. X-ray Structure Determination.** All software was from the CCP4 package<sup>50</sup> unless explicitly mentioned. The structure of Mcl-1 complexed with the BIM peptide was solved by molecular replacement using MolRep<sup>51</sup> using the published structure of Mcl-1 complexed with the BIM peptide (PDB code: 2NL9<sup>17</sup>) as a model. Subsequent Mcl-1 complexes were solved using the Mcl-1 model stripped of the peptide. The structure of the Bcl-2 complex with compound **1** was solved by molecular replacement using MolRep using the published crystal structure of Bcl-x<sub>L</sub> complexed with ABT-737 (PDB code 2YXJ<sup>19</sup>) stripped of the compound and solvent. From initial electron density maps, it became apparent that **1** is present in the binding site of Bcl-2. Initial maps allowed extension of the refinement resolution range and correct placement of side chains. At this point, differences between the Bcl-2 and Bcl-x<sub>L</sub> sequence were clearly visible, and appropriate changes were made in the model. In all cases, the refined structure of the relevant protein (stripped of the compound) was used as a starting model for solving by molecular replacement subsequent structures of the complexes of Mcl-1 or Bcl-2 with ligands. After structure solution, several cycles of refinement were conducted with Refmac5<sup>52</sup> software from the CCP4 package, alternating with manual rebuilding using the program COOT.<sup>53</sup> Compounds were modeled in the surplus peaks in difference Fourier electron density maps. Topology files for the ligands were created by ProDrg<sup>54</sup> (also from CCP4 package). Refinement statistics for each new structure reported in this paper are in Table S2.

## ■ ASSOCIATED CONTENT

### Supporting Information

The Supporting Information is available free of charge on the ACS Publications website at DOI: [10.1021/acsomega.9b00611](https://doi.org/10.1021/acsomega.9b00611).

Supplementary figures and tables and description of compound synthesis ([PDF](#))

Atomic coordinates and experimental data for all X-ray crystal structures and the atomic coordinates for NMR-guided models ([PDB](#))

## ■ AUTHOR INFORMATION

### Corresponding Author

\*E-mail: [r.hubbard@vernalis.com](mailto:r.hubbard@vernalis.com).

### ORCID

James B. Murray: [0000-0003-1007-8218](https://orcid.org/0000-0003-1007-8218)

Pawel Dokurno: [0000-0002-7332-8889](https://orcid.org/0000-0002-7332-8889)

Allan Jordan: [0000-0003-3449-3993](https://orcid.org/0000-0003-3449-3993)

Stephen D. Roughley: [0000-0003-0683-5693](https://orcid.org/0000-0003-0683-5693)

Yikang Wang: [0000-0002-1357-1377](https://orcid.org/0000-0002-1357-1377)

Douglas S. Williamson: [0000-0002-5094-5200](https://orcid.org/0000-0002-5094-5200)

András Kotschy: [0000-0002-7675-3864](https://orcid.org/0000-0002-7675-3864)

Roderick E. Hubbard: [0000-0002-8233-7461](https://orcid.org/0000-0002-8233-7461)

### Present Address

<sup>1</sup>Sygnature Discovery, Discovery Building, BioCity, Pennyfoot Street, Nottingham, NG1 1GR, U.K.

### Author Contributions

J.B.M. and J.D. contributed equally. The manuscript was written through contributions of all the authors. All the authors have given approval to the final version of the manuscript.

### Notes

The authors declare no competing financial interest.

## ■ ACKNOWLEDGMENTS

The authors thank Heather Simmonite and Loic Le Strat for analytical support at Vernalis and the industry liaison teams at the ESRF and Diamond synchrotrons for their help and assistance with X-ray data collection.

## ■ ABBREVIATIONS

AIS, affinity in solution; Bad, Bcl-2-associated death factor; Bak, Bcl-2 homologous antagonist killer; Bax, Bcl-2-associated X protein; Bcl-2, B-cell lymphoma 2; Bcl-w, Bcl-2-like protein 2; Bcl-x<sub>L</sub>, B-cell lymphoma extra large; Bfl-1, Bcl-2-related protein A1; BH3, Bcl-2 homology domain 3; Bim, Bcl-2-like protein 11; FP, fluorescence polarization; Hrk, activator of apoptosis Harakiri; ITC, isothermal titration calorimetry; Mcl-1, myeloid chronic leukemia 1; Noxa, phorbol-12-myristate-13-acetate-induced protein 1; Puma, p53 upregulated modulator of apoptosis; SPR, surface plasmon resonance

## ■ REFERENCES

- (1) Juin, P.; Geneste, O.; Gautier, F.; Depil, S.; Campone, M. Decoding and unlocking the BCL-2 dependency of cancer cells. *Nat. Rev. Cancer* **2013**, *13*, 455–465.
- (2) Wells, J. A.; McClendon, C. L. Reaching for high-hanging fruit in drug discovery at protein-protein interfaces. *Nature* **2007**, *450*, 1001–1009.
- (3) Yap, J. L.; Chen, L.; Lanning, M. E.; Fletcher, S. Expanding the Cancer Arsenal with Targeted Therapies: Disarmament of the

Antia apoptotic Bcl-2 Proteins by Small Molecules. *J. Med. Chem.* **2017**, *60*, 821–838.

(4) Souers, A. J.; Leverson, J. D.; Boghaert, E. R.; Ackler, S. L.; Catron, N. D.; Chen, J.; Dayton, B. D.; Ding, H.; Enschede, S. H.; Fairbrother, W. J.; Huang, D. C. S.; Hymowitz, S. G.; Jin, S.; Khaw, S. L.; Kovar, P. J.; Lam, L. T.; Lee, J.; Maecker, H. L.; Marsh, K. C.; Mason, K. D.; Mitten, M. J.; Nimmer, P. M.; Oleksijew, A.; Park, C. H.; Park, C.-M.; Phillips, D. C.; Roberts, A. W.; Sampath, D.; Seymour, J. F.; Smith, M. L.; Sullivan, G. M.; Tahir, S. K.; Tse, C.; Wendt, M. D.; Xiao, Y.; Xue, J. C.; Zhang, H.; Humerickhouse, R. A.; Rosenberg, S. H.; Elmore, S. W. ABT-199, a potent and selective BCL-2 inhibitor, achieves antitumor activity while sparing platelets. *Nat. Med.* **2013**, *19*, 202–208.

(5) Tse, C.; Shoemaker, A. R.; Adickes, J.; Anderson, M. G.; Chen, J.; Jin, S.; Johnson, E. F.; Marsh, K. C.; Mitten, M. J.; Nimmer, P.; Roberts, L.; Tahir, S. K.; Xiao, Y.; Yang, X.; Zhang, H.; Fesik, S.; Rosenberg, S. H.; Elmore, S. W. ABT-263: a potent and orally bioavailable Bcl-2 family inhibitor. *Cancer Res.* **2008**, *68*, 3421–3428.

(6) Oltersdorf, T.; Elmore, S. W.; Shoemaker, A. R.; Armstrong, R. C.; Augeri, D. J.; Belli, B. A.; Bruncko, M.; Deckwerth, T. L.; Dinges, J.; Hajduk, P. J.; Joseph, M. K.; Kitada, S.; Korsmeyer, S. J.; Kunzer, A. R.; Letai, A.; Li, C.; Mitten, M. J.; Nettelesheim, D. G.; Ng, S.; Nimmer, P. M.; O'Connor, J. M.; Oleksijew, A.; Petros, A. M.; Reed, J. C.; Shen, W.; Tahir, S. K.; Thompson, C. B.; Tomaselli, K. J.; Wang, B.; Wendt, M. D.; Zhang, H.; Fesik, S. W.; Rosenberg, S. H. An inhibitor of Bcl-2 family proteins induces regression of solid tumours. *Nature* **2005**, *435*, 677–681.

(7) Johannes, J. W.; Bates, S.; Beigie, C.; Belmonte, M. A.; Breen, J.; Cao, S.; Centrella, P. A.; Clark, M. A.; Cuozzo, J. W.; Dumelin, C. E.; Ferguson, A. D.; Habeshian, S.; Hargreaves, D.; Joubran, C.; Kazmirski, S.; Keefe, A. D.; Lamb, M. L.; Lan, H.; Li, Y.; Ma, H.; Mlynarski, S.; Packer, M. J.; Rawlins, P. B.; Robbins, D. W.; Shen, H.; Sigel, E. A.; Soutter, H. H.; Su, N.; Troast, D. M.; Wang, H.; Wickson, K. F.; Wu, C.; Zhang, Y.; Zhao, Q.; Zheng, X.; Hird, A. W. Structure Based Design of Non-Natural Peptidic Macrocyclic Mcl-1 Inhibitors. *ACS Med. Chem. Lett.* **2017**, *8*, 239–244.

(8) Zhao, B.; Sensintaffar, J.; Bian, Z.; Belmar, J.; Lee, T.; Olejniczak, E. T.; Fesik, S. W. Structure of a Myeloid cell leukemia-1 (Mcl-1) inhibitor bound to drug site 3 of Human Serum Albumin. *Bioorg. Med. Chem.* **2017**, *25*, 3087–3092.

(9) Caenepeel, S. R.; Belmontes, B.; Sun, J.; Coxon, A.; Moody, G.; Hughes, P. E. Abstract 2027: Preclinical evaluation of AMG 176, a novel, potent and selective Mcl-1 inhibitor with robust anti-tumor activity in Mcl-1 dependent cancer models. *Cancer Res.* **2017**, *77*, 2027.

(10) Casara, P.; Davidson, J.; Claperon, A.; Toumelin-Braizat, G. L.; Vogler, M.; Bruno, A.; Chanrion, M.; Lysiak-Auvity, G.; Diguarher, T. L.; Starck, J.-B.; Chen, I.; Whitehead, N.; Graham, C.; Matassova, N.; Dokurno, P.; Pedder, C.; Wang, Y.; Qiu, S.; Girard, A.-M.; Schneider, E.; Gravé, F.; Studeny, A.; Guasconi, G.; Rocchetti, F.; Maïga, S.; Henlin, J.-M.; Colland, F.; Kraus-Berthier, L.; Gouill, S. L.; Dyer, M. J.; Hubbard, R.; Wood, M.; Amiot, M.; Cohen, G. M.; Hickman, J. A.; Morris, E.; Murray, J.; Geneste, O. S55746 is a novel orally active BCL-2 selective and potent inhibitor that impairs hematological tumor growth. *Oncotarget* **2018**, *9*, 20075–20088.

(11) Kotschy, A.; Szlavik, Z.; Murray, J.; Davidson, J.; Maragno, A. L.; Le Toumelin-Braizat, G.; Chanrion, M.; Kelly, G. L.; Gong, J.-N.; Moujalled, D. M.; Bruno, A.; Csekei, M.; Paczal, A.; Szabo, Z. B.; Sipos, S.; Radics, G.; Proszenyak, A.; Balint, B.; Ondi, L.; Blasko, G.; Robertson, A.; Surgenor, A.; Dokurno, P.; Chen, I.; Matassova, N.; Smith, J.; Pedder, C.; Graham, C.; Studeny, A.; Lysiak-Auvity, G.; Girard, A.-M.; Gravé, F.; Segal, D.; Riffkin, C. D.; Pomilio, G.; Galbraith, L. C. A.; Aubrey, B. J.; Brennan, M. S.; Herold, M. J.; Chang, C.; Guasconi, G.; Cauquil, N.; Melchiore, F.; Guigal-Stephan, N.; Lockhart, B.; Colland, F.; Hickman, J. A.; Roberts, A. W.; Huang, D. C. S.; Wei, A. H.; Strasser, A.; Lessene, G.; Geneste, O. The MCL1 inhibitor S63845 is tolerable and effective in diverse cancer models. *Nature* **2016**, *538*, 477–482.

- (12) Szlávík, Z.; Ondi, L.; Csékei, M.; Paczal, A.; Szabó, Z. B.; Radics, G.; Murray, J.; Davidson, J.; Chen, I.; Davis, B.; Hubbard, R. E.; Pedder, C.; Dokurno, P.; Surgenor, A.; Smith, J.; Robertson, A.; LeToumelin-Braizat, G.; Cauquil, N.; Zarka, M.; Demarles, D.; Perron-Sierra, F.; Geneste, O.; Kotschy, A. The structure guided discovery of a selective Mcl-1 inhibitor with cellularactivity. Submitted for publication.
- (13) Fire, E.; Gullá Stefano, V.; Grant Robert, A.; Keating Amy, E. Mcl-1–Bim complexes accommodate surprising point mutations via minor structural changes. *Protein Sci.* **2010**, *19*, 507–519.
- (14) Chen, L.; Willis, S. N.; Wei, A.; Smith, B. J.; Fletcher, J. I.; Hinds, M. G.; Colman, P. M.; Day, C. L.; Adams, J. M.; Huang, D. C. S. Differential targeting of prosurvival Bcl-2 proteins by their BH3-only ligands allows complementary apoptotic function. *Mol. Cell* **2005**, *17*, 393–403.
- (15) Muchmore, S. W.; Sattler, M.; Liang, H.; Meadows, R. P.; Harlan, J. E.; Yoon, H. S.; Nettesheim, D.; Chang, B. S.; Thompson, C. B.; Wong, S.-L.; Ng, S.-C.; Fesik, S. W. X-ray and NMR structure of human Bcl-xL, an inhibitor of programmed cell death. *Nature* **1996**, *381*, 335–341.
- (16) Petros, A. M.; Medek, A.; Nettesheim, D. G.; Kim, D. H.; Yoon, H. S.; Swift, K.; Matayoshi, E. D.; Oltersdorf, T.; Fesik, S. W. Solution structure of the antiapoptotic protein bcl-2. *Proc. Natl. Acad. Sci. U.S.A.* **2001**, *98*, 3012–3017.
- (17) Czabotar, P. E.; Lee, E. F.; van Delft, M. F.; Day, C. L.; Smith, B. J.; Huang, D. C. S.; Fairlie, W. D.; Hinds, M. G.; Colman, P. M. Structural insights into the degradation of Mcl-1 induced by BH3 domains. *Proc. Natl. Acad. Sci. U.S.A.* **2007**, *104*, 6217–6222.
- (18) Fischer, M.; Leech, A. P.; Hubbard, R. E. Comparative Assessment of Different Histidine-Tags for Immobilization of Protein onto Surface Plasmon Resonance Sensorschips. *Anal. Chem.* **2011**, *83*, 1800.
- (19) Lee, E. F.; Czabotar, P. E.; Smith, B. J.; Deshayes, K.; Zobel, K.; Colman, P. M.; Fairlie, W. D. Crystal structure of ABT-737 complexed with Bcl-xL: implications for selectivity of antagonists of the Bcl-2 family. *Cell Death Differ.* **2007**, *14*, 1711–1713.
- (20) Cheng, A. C.; Coleman, R. G.; Smyth, K. T.; Cao, Q.; Soulard, P.; Caffrey, D. R.; Salzberg, A. C.; Huang, E. S. Structure-based maximal affinity model predicts small-molecule druggability. *Nat. Biotechnol.* **2007**, *25*, 71–75.
- (21) Hajduk, P. J.; Bures, M.; Praestgaard, J.; Fesik, S. W. Privileged molecules for protein binding identified from NMR-based screening. *J. Med. Chem.* **2000**, *43*, 3443–3447.
- (22) Porter, J.; Payne, A.; de Candole, B.; Ford, D.; Hutchinson, B.; Trevitt, G.; Turner, J.; Edwards, C.; Watkins, C.; Whitcombe, I.; Davis, J.; Stubberfield, C. Tetrahydroisoquinoline amide substituted phenyl pyrazoles as selective Bcl-2 inhibitors. *Bioorg. Med. Chem. Lett.* **2009**, *19*, 230–233.
- (23) Elmore, S. W.; Souers, A. J.; Bruncko, M.; Song, X.; Hasvold, L. A.; Wang, L.; Kunzer, A. R.; Park, C.-M.; Wendt, M. D.; Tao, Z.-F. 7-Substituted indoles as MCL-1 protein inhibitors and their preparation. PCT Int. Appl. WO2008131000A2, 2008.
- (24) Bruncko, M.; Wang, L.; Sheppard, G. S.; Phillips, D. C.; Tahir, S. K.; Xue, J.; Erickson, S.; Fidanze, S.; Fry, E.; Hasvold, L.; Jenkins, G. J.; Jin, S.; Judge, R. A.; Kovar, P. J.; Madar, D.; Nimmer, P.; Park, C.; Petros, A. M.; Rosenberg, S. H.; Smith, M. L.; Song, X.; Sun, C.; Tao, Z.-F.; Wang, X.; Xiao, Y.; Zhang, H.; Tse, C.; Leverson, J. D.; Elmore, S. W.; Souers, A. J. Structure-Guided Design of a Series of MCL-1 Inhibitors with High Affinity and Selectivity. *J. Med. Chem.* **2015**, *58*, 2180–2194.
- (25) Chen, I.-J.; Hubbard, R. E. Lessons for fragment library design: analysis of output from multiple screening campaigns. *J. Comput.-Aided Mol. Des.* **2009**, *23*, 603–620.
- (26) Hajduk, P. J.; Huth, J. R.; Fesik, S. W. Druggability indices for protein targets derived from NMR-based screening data. *J. Med. Chem.* **2005**, *48*, 2518–2525.
- (27) Doak, B. C.; Morton, C. J.; Simpson, J. S.; Scanlon, M. J. Design and Evaluation of the Performance of an NMR Screening Fragment Library. *Aust. J. Chem.* **2013**, *66*, 1465.
- (28) Chilton, M.; Clennell, B.; Edfeldt, F.; Geschwindner, S. Hot-Spotting with Thermal Scanning: A Ligand- and Structure-Independent Assessment of Target Ligandability. *J. Med. Chem.* **2017**, *60*, 4923–4931.
- (29) Edfeldt, F. N. B.; Folmer, R. H. A.; Breeze, A. L. Fragment screening to predict druggability (ligandability) and lead discovery success. *Drug Discovery Today* **2011**, *16*, 284–287.
- (30) Pelz, N. F.; Bian, Z.; Zhao, B.; Shaw, S.; Tarr, J. C.; Belmar, J.; Gregg, C.; Camper, D. V.; Goodwin, C. M.; Arnold, A. L.; Sensintaffar, J. L.; Friberg, A.; Rossanese, O. W.; Lee, T.; Olejniczak, E. T.; Fesik, S. W. Discovery of 2-Indole-acylsulfonamide Myeloid Cell Leukemia 1 (Mcl-1) Inhibitors Using Fragment-Based Methods. *J. Med. Chem.* **2016**, *59*, 2054–2066.
- (31) Clifton, M. C.; Dranow, D. M.; Leed, A.; Fulroth, B.; Fairman, J. W.; Abendroth, J.; Atkins, K. A.; Wallace, E.; Fan, D.; Xu, G.; Ni, Z. J.; Daniels, D.; Van Drie, J.; Wei, G.; Burgin, A. B.; Golub, T. R.; Hubbard, B. K.; Serrano-Wu, M. H. A Maltose-Binding Protein Fusion Construct Yields a Robust Crystallography Platform for MCL1. *PLoS One* **2015**, *10*, No. e0125010.
- (32) Vranken, W. F.; Boucher, W.; Stevens, T. J.; Fogh, R. H.; Pajon, A.; Llinas, M.; Ulrich, E. L.; Markley, J. L.; Ionides, J.; Laue, E. D. The CCPN data model for NMR spectroscopy: development of a software pipeline. *Proteins* **2005**, *59*, 687–696.
- (33) Czabotar, P. E.; Lee, E. F.; van Delft, M. F.; Day, C. L.; Smith, B. J.; Huang, D. C. S.; Fairlie, W. D.; Hinds, M. G.; Colman, P. M. Structural insights into the degradation of Mcl-1 induced by BH3 domains. *Proc. Natl. Acad. Sci. U.S.A.* **2007**, *104*, 6217–6222.
- (34) Madhavi Sastry, G.; Adzhigirey, M.; Day, T.; Annabhimoju, R.; Sherman, W. Protein and ligand preparation: parameters, protocols, and influence on virtual screening enrichments. *J. Comput.-Aided Mol. Des.* **2013**, *27*, 221–234.
- (35) Sagui, C.; Darden, T. A. Molecular dynamics simulations of biomolecules: long-range electrostatic effects. *Annu. Rev. Biophys. Biomol. Struct.* **1999**, *28*, 155–179.
- (36) Bowers, K. J.; Chow, E.; Xu, H.; Dror, R. O.; Eastwood, M. P.; Gregersen, B. A.; Klepeis, J. L.; Kolossvary, I.; Moraes, M. A.; Sacerdoti, F. D.; Salmon, J. K.; Shan, Y.; Shaw, D. E. Scalable Algorithms for Molecular Dynamics Simulations on Commodity Clusters. *Proceedings of the ACM/IEEE Conference on Supercomputing (SC06)*, Tampa, Florida, 2006.
- (37) Case, D. A.; Darden, T. A.; Cheatham, T. E.; Simmerling, C. L.; Wang, J.; Duke, R. E.; Luo, R. C. W.; Zhang, W.; Merz, K. M.; Roberts, B.; Hayik, S.; Roitberg, A.; Seabra, G.; Swails, J.; Kolossváry, I.; Wong, K. F.; Paesani, F.; Vanicek, J.; Wolf, R. M.; Liu, J.; Wu, X.; Steinbrecher, T.; Gohlke, H.; Cai, Q.; Ye, X.; Wang, J.; Hsieh, M.-J.; Cui, D. R. R.; Mathews, D. H.; Seetin, M. G.; Salmon-Ferrer, R.; Sagui, C.; Babin, V.; Luchko, S. G.; Kovalenko, A.; Kollman, P. A. *Amber12*; University of California: San Francisco, 2012.
- (38) Onufriev, A.; Bashford, D.; Case, D. A. Modification of the Generalized Born Model Suitable for Macromolecules. *J. Phys. Chem. B* **2000**, *104*, 3712–3720.
- (39) Halgren, T. A.; Murphy, R. B.; Friesner, R. A.; Beard, H. S.; Frye, L. L.; Pollard, W. T.; Banks, J. L. Glide: a new approach for rapid, accurate docking and scoring. 2. Enrichment factors in database screening. *J. Med. Chem.* **2004**, *47*, 1750–1759.
- (40) Repasky, M. P.; Shelley, M.; Friesner, R. A. Flexible ligand docking with Glide. *Curr. Protoc. Bioinformatics* **2007**, *18*, 8.12.1.
- (41) Sherman, W.; Day, T.; Jacobson, M. P.; Friesner, R. A.; Farid, R. Novel procedure for modeling ligand/receptor induced fit effects. *J. Med. Chem.* **2006**, *49*, 534–553.
- (42) Nikolovska-Coleska, Z.; Wang, R.; Fang, X.; Pan, H.; Tomita, Y.; Li, P.; Roller, P. P.; Krajewski, K.; Saito, N. G.; Stuckey, J. A.; Wang, S. Development and optimization of a binding assay for the XIAP BIR3 domain using fluorescence polarization. *Anal. Biochem.* **2004**, *332*, 261–273.
- (43) Baurin, N.; Aboul-Ela, F.; Barril, X.; Davis, B.; Drysdale, M.; Dymock, B.; Finch, H.; Fromont, C.; Richardson, C.; Simonite, H.; Hubbard, R. E. Design and characterization of libraries of molecular

fragments for use in NMR screening against protein targets. *J. Chem. Inf. Comput. Sci.* **2004**, *44*, 2157–2166.

(44) Mayer, M.; Meyer, B. Characterization of Ligand Binding by Saturation Transfer Difference NMR Spectroscopy. *Angew. Chem., Int. Ed.* **1999**, *38*, 1784–1788.

(45) Dalvit, C.; Fogliatto, G.; Stewart, A.; Veronesi, M.; Stockman, B. WaterLOGSY as a method for primary NMR screening: practical aspects and range of applicability. *J. Biomol. NMR* **2001**, *21*, 349–359.

(46) Hajduk, P. J.; Olejniczak, E. T.; Fesik, S. W. One-Dimensional Relaxation- and Diffusion-Edited NMR Methods for Screening Compounds That Bind to Macromolecules. *J. Am. Chem. Soc.* **1997**, *119*, 12257–12261.

(47) Brough, P. A.; Barril, X.; Borgognoni, J.; Chene, P.; Davies, N. G.; Davis, B.; Drysdale, M. J.; Dymock, B.; Eccles, S. A.; Garcia-Echeverria, C.; Fromont, C.; Hayes, A.; Hubbard, R. E.; Jordan, A. M.; Jensen, M. R.; Massey, A.; Merrett, A.; Padfield, A.; Parsons, R.; Radimerski, T.; Raynaud, F. I.; Robertson, A.; Roughley, S. D.; Schoepfer, J.; Simmonite, H.; Sharp, S. Y.; Surgenor, A.; Valenti, M.; Walls, S.; Webb, P.; Wood, M.; Workman, P.; Wright, L. Combining hit identification strategies: fragment-based and *in silico* approaches to orally active 2-aminothieno[2,3-d]pyrimidine inhibitors of the Hsp90 molecular chaperone. *J. Med. Chem.* **2009**, *52*, 4794–4809.

(48) Otwinowski, Z.; Minor, W. DENZO and SCALEPACK. In *International Tables for Crystallography Volume F: Crystallography of Biological Macromolecules*; Rossmann, M. G., Arnold, E., Eds.; Springer Netherlands: Dordrecht, 2001; pp 226–235.

(49) Pflugrath, J. W. The finer things in X-ray diffraction data collection. *Acta Crystallogr., Sect. D: Biol. Crystallogr.* **1999**, *55*, 1718–1725.

(50) Winn, M. D.; Ballard, C. C.; Cowtan, K. D.; Dodson, E. J.; Emsley, P.; Evans, P. R.; Keegan, R. M.; Krissinel, E. B.; Leslie, A. G. W.; McCoy, A.; McNicholas, S. J.; Murshudov, G. N.; Pannu, N. S.; Potterton, E. A.; Powell, H. R.; Read, R. J.; Vagin, A.; Wilson, K. S. Overview of the CCP4 suite and current developments. *Acta Crystallogr., Sect. D: Biol. Crystallogr.* **2011**, *67*, 235–242.

(51) Vagin, A.; Teplyakov, A. Molecular replacement with MOLREP. *Acta Crystallogr., Sect. D: Biol. Crystallogr.* **2010**, *66*, 22–25.

(52) Murshudov, G. N.; Vagin, A. A.; Dodson, E. J. Refinement of macromolecular structures by the maximum-likelihood method. *Acta Crystallogr., Sect. D: Biol. Crystallogr.* **1997**, *53*, 240–255.

(53) Emsley, P.; Cowtan, K. Coot: model-building tools for molecular graphics. *Acta Crystallogr., Sect. D: Biol. Crystallogr.* **2004**, *60*, 2126–2132.

(54) Schüttelkopf, A. W.; van Aalten, D. M. F. PRODRG: a tool for high-throughput crystallography of protein-ligand complexes. *Acta Crystallogr., Sect. D: Biol. Crystallogr.* **2004**, *60*, 1355–1363.